JGR Oceans

RESEARCH ARTICLE
10.1029/2020JC016673

Exploring the Roles of Iron and Irradiance in Dynamics of Diatoms and *Phaeocystis* in the Amundsen Sea Continental Shelf Water

Young Shin Kwon[1,2], Hyoung Sul La[1], Jinyoung Jung[1], Sang Heon Lee[3], Tae-Wan Kim[1], Hyoun-Woo Kang[4], and SangHoon Lee[1]

[1]Division of Ocean Sciences, Korea Polar Research Institute, Incheon, Korea, [2]Department of Polar Science, University of Science and Technology, Daejeon, Korea, [3]Department of Oceanography, Pusan National University, Busan, Korea, [4]Marine Environment and Climate Research Division, Korea Institute of Ocean Science and Technology, Busan, Korea

Key Points:

- One-dimensional physical-biogeochemical model successfully reproduced key ecodynamics of diatoms and *Phaeocystis* in the Amundsen Sea
- Current moderate iron availability and excessive light conditions in the Amundsen Sea favor *Phaeocystis* over diatoms, which would persist
- Net primary production of the Amundsen Sea could increase with increasing ice sheets melt in the future

Supporting Information:

- Supporting Information S1

Correspondence to:
H. S. La,
hsla@kopri.re.kr

Citation:
Kwon, Y. S., La, H. S., Jung, J., Lee, S. H., Kim, T.-W., Kang, H.-W., & Lee, S. (2021). Exploring the roles of iron and irradiance in dynamics of diatoms and *Phaeocystis* in the Amundsen Sea continental shelf water. *Journal of Geophysical Research: Oceans*, *126*, e2020JC016673. https://doi.org/10.1029/2020JC016673

Received 1 AUG 2020
Accepted 14 JAN 2021

Abstract The Amundsen Sea continental shelf (ACS) water ecosystem is expected to undergo changes since increasing melt rate of glacier and decreasing sea ice extent by global warming would lead to the mitigation of iron and light limitation. We investigated how diatoms and *Phaeocystis*, two dominant taxa, and primary production in the ACS water would respond to variations in iron and light availabilities by using a 1-D pelagic ecosystem model. In the model, we added sea ice effects that reduce light penetration and optimized model parameters for diatoms and *Phaeocystis*. The results from our model showed good agreement with 20-year observations of Chl-*a* as well as the biomass proportion of diatoms and *Phaeocystis* and nutrient distributions during the growing season. Our model experimental results suggest that the current moderate iron and high light conditions favor the growth of *Phaeocystis* over diatoms. Moreover, as iron increases, the organic carbon exudation by phytoplankton increases more rapidly than net primary production (NPP), leading to a decline in phytoplankton biomass. On the other hand, irradiance plays a role in controlling NPP in terms of photoinhibition which is reduced by increasing iron. Increases in both iron and irradiance lead to an advance in the timing of the bloom peak (surface Chl-*a* maximum) due to increases in phytoplankton carbon loss and photoinhibition. Our results imply that the dominance of *Phaeocystis* can continue and that the carbon uptake capacity of the ACS in the summer seasons might increase given that iron availability will increase with future climate change.

Plain Language Summary We firmly believe that this research based on an optimum biogeochemical model developed for the Amundsen Sea continental shelf water is of sufficiently broad interest for the public as well as the scientific community, since it advances the study of phytoplankton ecology and carbon uptake in the Antarctic coastal area. A complex coupled ocean-ecosystem model was developed to investigate dynamics of the two dominant species (diatoms and *Phaeocystis*) in the ACS water, one of the most rapidly warming regions on Earth with extremely high primary productivity. These two groups are particularly important as they could significantly contribute to the carbon export into the deep ocean. The model is able to accurately address the temporal evolution of diatoms and *Phaeocystis* responding to the variations of nutrients, iron, and irradiance. We show these two groups of phytoplankton are controlled by the rate of irradiance and iron availability in terms of the net primary production (NPP), biomass contribution, and bloom period. This research presents new evidence that the short-term export production of *Phaeocystis*-derived carbon can become stronger in the future with increasing basal melt in the coastal waters around the Antarctic continent.

1. Introduction

The Southern Ocean, generally defined as the waters occurring south of 60°S and encircling Antarctica, plays a disproportionate role in control of atmospheric carbon by contributing ~40% of the total oceanic uptake of anthropogenic carbon dioxide (CO_2) emissions (Frölicher et al., 2015; Khatiwala et al., 2009; Takahashi et al., 2009, 2012). In particular, the Antarctic continental shelf areas show substantial carbon uptake capacity due to efficient biological pump through primary production (Arrigo et al., 2008) during the summertime when sea ice retreat allows solar irradiance penetration into the upper ocean. However, the reason for the low efficiency of carbon export into the deep ocean despite the high productivity in the upper

layers are unclear but have been recognized from the moored sediment trap data (Ducklow et al., 2015; S. Lee et al., 2017). Although there are exceptions such as the Western Antarctic Peninsula (WAP), where other small species are also dominant (e.g., Brown et al., 2019), much of the primary production in these areas is carried out by diatoms and *Phaeocystis antarctica* (as *Phaeocystis* below) (Alderkamp et al., 2012b; Annett et al., 2010; Arrigo et al., 1999; Davidson & Marchant, 1992; Delmont et al., 2014; G. R. DiTullio & Smith, 1996; Garibotti et al., 2005; T. Moisan & Fryxell, 1993; Nothig et al., 1991; Waters et al., 2000; Wright & van den Enden, 2000).

The Amundsen Sea continental shelf (ACS) is known to have the highest primary production per unit area around Antarctica during the growing season (Arrigo & van Dijken, 2003). In terms of the primary production, the Antarctic coastal regions, including the ACS share two common environmental features: 1) extreme variation in the solar irradiance depending on seasonal changes and the sea ice extent and 2) seasonally iron-depleted condition for the primary production. However, these tendencies could be perturbed by future environmental changes, especially the acceleration of basal melting of ice shelves by increasing intrusion of circumpolar deep water (CDW; Deb et al., 2018), the warming of sea surface water (Schmidtko et al., 2014), increased nutrient input by enhanced coastal upwelling (Moore et al., 2018), and intensified stratification by the rapid melting of ice sheets (Arrigo et al., 2015). Reductions in ice sheets and sea ice and weakened vertical mixing can increase the availability of iron and light in this area, which is expected to impact lower-trophic-level biota (Boyd & Brown, 2015; Boyd et al., 2016; Brown et al., 2019). On the other hand, the increase in the exposure duration of the upper pelagic layer to the atmosphere with the increasing sea ice retreat might play a role in reducing light availability or increasing nutrients (e.g., iron) supply into the euphotic depth by inducing intermittent wind-driven mixing (Schultz et al., 2020).

Many previous studies have reported contrasting physiological and biogeochemical properties of the two species, especially in response to the iron concentration and irradiance level: generally, while *Phaeocystis* is known to be better adapted to lower irradiance levels than diatoms (Arrigo et al., 1999, 2000, 2010; G. DiTullio et al., 2000; T. A. Moisan et al., 1998; Rogers et al., 2019; Schoemann et al., 2005; Sedwick et al., 2000), diatoms which have significantly low iron requirements and are reported to be effectively acclimated to low-iron conditions (Hoffmann et al., 2006; Strzepek & Harrison, 2004; Strzepek et al., 2011; Sunda et al., 1991). Additionally, diatoms and *Phaeocystis* differ in terms of intracellular stoichiometry and export processes (Arrigo et al., 1999; Asper & Smith, 1999). *Phaeocystis* is known to have higher cellular carbon ratios than diatoms (Arrigo et al., 1999) and the cellular carbon content of *Phaeocystis* colonies can be higher than that of single cells during blooms (Solomon et al., 2003). Under the Nutrient-replete conditions, the stoichiometry of *Phaeocystis* is known to be closer to the Redfield ratio (Schoemann et al., 2005). Therefore, shifts in phytoplankton dominance due to environmental changes will impact the biological pump in this area.

However, there is considerable debate about the responses of the two species to these environmental changes (Deppeler & Davidson, 2017). Although several studies on the individual or interactive roles of iron and light have been conducted (Boyd et al., 2015; Feng et al., 2010; Sedwick et al., 2007; Strzepek et al., 2019; Sunda & Huntsman, 1997), there is a lack of consensus regarding the dynamics that govern the productivity in this area. Moreover, still the observations and laboratory incubation experiments on the roles of temperature, grazing rate by predators, and acidification are deficient (e.g., Jabre & Bertrand, 2020). Hence, predicting the responses of ecosystems to environmental changes is not straightforward currently. Modeling studies can provide a valuable complement to field measurements in this regard. To the best of our knowledge, although there have been several modeling studies on the Ross Sea (Arrigo et al., 2003; Coale et al., 2003; Pasquer et al., 2005), there is only two studies applied an ecosystem model for the ACS water (Oliver et al., 2019; St-Laurent et al., 2019) and only considered the *Phaeocystis* group, not diatoms. Although the model results of Oliver et al. (2019) suggested that phytoplankton self-shading limits the primary production in the summer, their relatively simplified model did not consider the effects of varying cellular carbon with Chlorophyll-*a* (Chl-*a*) ratio and iron availability on light limitation level. As the rate of light absorption is proportional to the Chl-*a* content of the cells (Geider et al., 1998), the cells with high Chl-*a* content are favored under low light condition while more susceptible to the photoinhibition under excessive light conditions (Van De Poll et al., 2005; Van Leeuwe & Stefels, 2007). The main species of the Southern Ocean are known to have strategies to adjust to the ambient light levels depending on the concentration of iron (e.g., Strzepek et al., 2011), an essential element for the electron transfer reactions of photosynthesis

(Doucette & Harrison, 1990; Geider et al., 1993). In addition, the possible variation in the initial slope of the *P-I* curve depending on the iron concentration was not considered in their model, and it might significantly impact the results (Alderkamp et al., 2015; Strzepek et al., 2019). In this study, we adopted the European Regional Seas Ecosystem Model (ERSEM), a highly elaborate lower-trophic-level marine ecosystem model (Butenschön et al., 2016), to address questions concerning with the influences of iron and irradiance on the productivity in the ACS water.

We report on model enhancement and model experiments focusing on phytoplankton dynamics in the ACS region. Using the ERSEM coupled with a one-dimensional (1-D) vertical water column model (GOTM; General Ocean Turbulence Model), we enhanced the model by incorporating the effects of sea ice reducing light penetration and air-sea gas exchange through the sea surface; we considered both diatoms and *Phaeocystis* as phytoplankton functional groups and optimized their parameters. For the parameter optimization, we used the satellite-derived surface Chl-*a* and biomass proportions of diatoms and *Phaeocystis* from the in situ measurements. The model output was evaluated against the observed data sets that were not used for the optimization (net primary production [NPP] and vertical distributions of nutrients and Chl-*a*) as well as those used for the optimization. Using our enhanced model, we analyzed the responses of the phytoplankton ecosystem to variations in iron and irradiance. Based on these model results, we investigated the roles of the iron and irradiance and their interactive effects on productivity and the biomass proportion of diatoms and *Phaeocystis* in the Amundsen Sea. This study elucidates the precise mechanism of the carbon uptake capacity in the Amundsen Sea with the variations in iron and irradiance and to qualitatively assess the roles of this area in terms of the global climate change.

2. Model Description

We adopted a lower-trophic-level marine ecosystem model coupled with a 1-D vertical mixing model, the ERSEM-GOTM (Allen et al., 2004). GOTM, a 1-D ocean water column model, implements several standard turbulence closure schemes for vertical turbulent exchange processes in the marine environment (Burchard & Petersen, 1999; http://www.gotm.net). The standard ERSEM consists of several major biogeochemical/ecosystem compartments: four phytoplankton functional groups, three zooplankton functional groups, one heterotrophic bacteria functional group, dissolved/particulate organic matter, dissolved oxygen, inorganic carbon species, and nutrients (nitrate, ammonium, phosphate, iron, and dissolved silicon). The particulate organic matter is treated in three size classes (small, medium, and large) in relation to its origin, with different sinking rates (1, 5, and 10 m d^{-1}, respectively). Since a key feature of ERSEM is the decoupling of carbon and nutrient dynamics, it can be a powerful tool to understand the marine carbon cycle. Details of this complex model not provided in this paper are fully explained in Butenschön et al. (2016).

2.1. Incorporation of Sea Ice Effects

One of our model enhancement strategies is to incorporate the effects of sea ice existence on the lower-trophic-level ecosystem. To calculate sea ice albedo, the linear relationship between sea ice concentration and all-wave albedo, which Allison et al. (1993) reported, was adopted. The sea ice albedo, A, can be expressed as a linear function of F_{ice} (0–1), the ice concentration:

$$A = F_{ice}a + b \tag{1}$$

where a and b were determined to be 0.55 and 0.07, respectively, the mean slope values of the data sets in Allison et al. (1993). Sea ice reflects the incident light on the surface layer (I_0^+) by $A \cdot I_0^+$. Therefore, I_0^-, the light penetrating through the sea ice into the water column, can be expressed as

$$I_0 = \left(1 - A\right) I_0^+ \tag{2}$$

Comparing the averaged surface irradiance in summer seasons (December to February) over the 20 years, we obtained a 30% reduction in light penetration and a one-month delayed peak irradiance compared with the result without this albedo effect (Figure S1).

Second, the air-sea gas and heat exchanges were modified by making them inversely proportionate to the fractional ice cover following the literature (Hood et al., 1999; Tortell et al., 2011).

We used the sea ice concentration from the European Centre for Medium-Range Weather Forecast Reanalysis data (ERA-interim; Dee et al., 2011) to calculate the sea ice albedo and the gas blocking factor (for CO_2 and O_2) and heat fluxes at the sea surface.

We expect that model relaxation toward the observed temperature and salinity (T/S) in the summer and winter seasons would replace the effect of the surface freshwater flux, which is more accurate than attempting to specify freshwater flux.

Among several potential effects of sea ice on the pelagic ecosystem, we do not consider the variation in iron concentration induced by sea ice melting and the biogeochemistry of the sea ice ecosystem (e.g., ice algal dynamics). The former is known to be minor (Gerringa et al., 2012) and the latter has many debatable aspects because the sea ice ecosystem has been barely studied.

2.2. Modification of the Model Parameters for Phytoplankton in the ACS Water

In the model, while all phytoplankton functional types (PFTs) are considered to have similar life cycles overall, they have differences in terms of their physiological properties, such as adaptation to ambient light and nutrient availability (Butenschön et al., 2016). These differences are represented by a variety of model parameters used for their dynamics. Along with diatoms, *Phaeocystis*, a widely distributed species in the Southern Ocean, can be very competitive during the growing season (Ducklow et al., 2015; Yager et al., 2016). In this study, this species was newly incorporated into the ERSEM in this study to investigate the competition between diatoms and *Phaeocystis*. If we adopt the standard parameters from Butenschön et al. (2016) without any modifications, the phytoplankton composition is not realistic as small PFTs (nanophytoplankton and picophytoplankton) dominate the ecosystem (Figure S2). To make the parameters appropriate for the ACS water ecodynamics, we modified the microphytoplankton group to represent *Phaeocystis* (as a colony), by optimizing its physiological parameters. Additionally, we modified the parameters for diatoms and small species dynamics. The transformation of *Phaeocystis* between the solitary and colonial phases is not considered since the majority of *Phaeocystis* blooms as a colony in the Amundsen Sea (Schoemann et al., 2005). We chose the parameters for the *Phaeocystis* group following the observed features of its colonies. Following Wang and Moore (2011), we considered the single cells of *Phaeocystis* as part of the small PFTs. The important equations related to phytoplankton dynamics are provided in detail in Text S1 (supporting information). To avoid confusion, we use the symbols L_i, L_T, L_{NP}, L_{Fe}, and L_S to refer to the limitation factors governing the phytoplankton biomass specific growth rate, namely, the light, temperature, macronutrients, iron, and silicate limitation factor, respectively. L_i is influenced by multiple factors of the surface irradiance, the self-shading effect by particles and phytoplankton itself within the water column, and the iron concentration (Equation S4). The nutrient limitation factors, L_{NP}, L_{Fe}, and L_S, are all determined by their ambient concentrations in the model. The limitation factors vary between 0 (exhausted) and 1 (replete). The limitation factor is "high" when the limitation is weak and "low" when the limitation is strong.

Although there are numerous parameters concerning with the phytoplankton physiological/biogeochemical processes in the model, we focused on those directly affecting the growth rate for the parameter optimization. Given that physiological controls rather than biogeochemical processes contribute more to the model fit to the data (Oliver et al., 2019), we chose the parameters required to be recalibrated including the initial slope of the *P-I* curve (α), the half-saturation concentrations of nutrients (k_{Fe}, k_N, k_P, and k_S), the maximal growth rate (g_{max}), and the maximal effective Chl-*a* to carbon photosynthesis ratio (θ_{max}).

Because it is indisputable that *Phaeocystis* has higher α values than diatoms (Arrigo et al., 2010; Kropuenske et al., 2010), we regarded α^P as an ~2.5 times higher value than α^D following Wang and Moore (2011) (Table 1). Although Strzepek et al. (2019) reported that α can be sensitive to iron concentration, it was not considered in this study, as the range of iron concentration in their experiment (~0.145 nM) was much lower than the present level of the Amundsen Sea (~0.3 nM; Sherrell et al., 2015). The photoinhibition parameter β was determined to be twice as high for *Phaeocystis* than for diatoms according to the observations of Arrigo et al. (2010). The light attenuation in the water column in the model is briefly explained in Text S2 (supporting information) and important parameters are given in Table 1. Half-saturation values for nitrate,

Table 1
Important Model Parameters for the Phytoplankton Functional Groups and Iron Cycle

Parameter	Value	Unit	Description	Remarks
α^S	3.363	mg m^2 W^{-1} d^{-1}	Initial slope of *P-I* curve for small phytoplankton	Wang and Moore (2011)
α^D	3.003		Initial slope of *P-I* curve for diatoms	
α^P	7.566		Initial slope of *P-I* curve for *Phaeocystis*	
β^S	0.1	mg m^2 W^{-1} d^{-1}	Photoinhibition parameter for small phytoplankton	Arrigo et al. (2010)
β^D	0.1		Photoinhibition parameter for diatoms	
β^P	0.2		Photoinhibition parameter for *Phaeocystis*	
$k_N{}^S$	0.5	μM	Half-saturation constant for nitrate limitation of small phytoplankton	Wang and Moore (2011)
$k_P{}^S$	0.01		Half-saturation constant for phosphate limitation of small phytoplankton	
$k_N{}^D$	2.5		Half-saturation constant for nitrate limitation of diatoms	
$k_P{}^D$	0.1		Half-saturation constant for phosphate limitation of diatoms	
k_S	1		Half-saturation constant for silicate limitation of diatoms	
$k_N{}^P$	2.5		Half-saturation constant for nitrate limitation of *Phaeocystis*	
$k_P{}^P$	0.1		Half-saturation constant for phosphate limitation of *Phaeocystis*	
$r_{mort}{}^{S,D,P}$	0.05	d^{-1}	Specific mortality of phytoplankton at reference temperature (10°C)	The same mortality rate for all species
Sr^D	5	m d^{-1}	Maximal sinking velocity of diatoms	Default value of Butenschön et al. (2016)
Sr^P	5		Maximal sinking velocity of *Phaeocystis*	
$Pr_{Z5}{}^{Z5}$	0.1	1	Food preference of microzooplankton for microzooplankton	The same grazing rate for *Phaeocystis* and diatoms
$Pr_P{}^{Z5}$	0.15		Food preference of microzooplankton for *Phaeocystis*	
$Pr_D{}^{Z5}$	0.15		Food preference of microzooplankton for diatoms	
r_{scav}	0.00007	d^{-1}	Specific scavenging rate for iron	Default value of Butenschön et al. (2016)
q_M	1.0		Turn-over rate of dissolved organic matter (including iron) by bacteria	
$g_{max}{}^B$	2.2		Maximum specific uptake of bacteria at reference temperature	
a_{sea}	0.03	m^{-1}	Adsorption coefficient of clear water	
a_R	0.00001	m^2 mg^{-2}	Specific adsorption coefficient of particulate organic carbon	
a^D	0.007	m^2 mg^{-2}	Specific adsorption coefficient of diatoms	
a^{nano}	0.0041	m^2 mg^{-2}	Specific adsorption coefficient of nanophytoplankton	
a^{pico}	0.023	m^2 mg^{-2}	Specific adsorption coefficient of picophytoplankton	
a^P	0.008	m^2 mg^{-2}	Specific adsorption coefficient of Phaeocystis	

Note. The superscripts S, D, and P denote small species, diatoms, and *Phaeocystis*, respectively. As nano- and picophytoplankton had the same parameter values, we marked them together as small phytoplankton.

phosphate, and silicate were taken from Wang and Moore (2011). For the mortality rate of *Phaeocystis*, we adopted the value of diatoms of the standard ERSEM (Butenschön et al., 2016) because we had little information on the phytoplankton mortality rate in the Southern Ocean. Contrary to the small species floating in the upper ocean during their whole life cycle, diatoms and *Phaeocystis* are presumed to undergo sedimentation due to their large cellular sizes. There are no observed data on the food preference of consumers in the Amundsen Sea and therefore we assigned the same preference of microzooplankton and mesozooplankton for diatoms and *Phaeocystis*.

Regarding k_{Fe}, g_{max}, and $\theta_{max,}$ there is still debate on the two species, and additionally, these parameters have extensive ranges of observation (Arrigo et al., 2010; Coale et al., 2003; Garcia et al., 2009; Kropuenske et al., 2009; Schoemann et al., 2005; Strzepek et al., 2011; Timmermans et al., 2004). These nine parameters in Table 2 were recalibrated by an optimization procedure.

Table 2
Model Parameters Optimized for the ACS Water

Parameter	Boundary range for optimization	Optimal value	Unit	Description	Remarks
g_{max}^{S}		0.97 ± 0.01	d^{-1}	Maximum specific productivity of small phytoplankton at reference temperature	60% of g_{max}^{D}
g_{max}^{D}	0.15–3	1.61 ± 0.04		Maximum specific productivity of diatoms at reference temperature	AR03, AU03, C03, L05, P05, W11
g_{max}^{P}	0.82–7.2	3.32 ± 0.20		Maximum specific productivity of *Phaeocystis* at reference temperature	AR03, C03, L05, P05, W11
k_{Fe}^{S}		0.022 ± 0.001	nM	Half-saturation constant for iron limitation of small phytoplankton	60% of k_{Fe}^{D}
k_{Fe}^{D}	0.02–0.35	0.037 ± 0.002		Half-saturation constant for iron limitation of diatoms	AR03, AU03, C03, L05, P05, W11
k_{Fe}^{P}	0.02–0.35	0.298 ± 0.020		Half-saturation constant for iron limitation of *Phaeocystis*	AR03, C03, L05, P05, W11
θ_{max}^{S}		0.028 ± 0.001	mg Chl (mg C)$^{-1}$	Maximal effective chlorophyll to carbon photosynthesis ratio of small phytoplankton	60% of θ_{max}^{D}
θ_{max}^{D}	0.016–0.06	0.047 ± 0.001		Maximal effective chlorophyll to carbon photosynthesis ratio of diatoms	AR03, AU03, L05, W11
θ_{max}^{P}	0.01–0.04	0.024 ± 0.001		Maximal effective chlorophyll to carbon photosynthesis ratio of *Phaeocystis*	AR03, L05, W11

Note. The upper and lower bounds for the parameter optimization were determined based on the literature in the Remarks column. AR03 denotes Arrigo et al. (2010), AU03 denotes Aumont et al. (2003), C03 denotes Coale et al. (2003), L05 denotes Lancelot et al. (2005), P05 denotes Pasquer et al. (2005), and W11 denotes Wang and Moore (2011).

For the optimization, we first defined an objective function as the root-mean-square-error (RMSE) for the surface Chl-*a*. Since running the model to calculate the RMSE during parameter tuning is a time-intensive process, we chose to use Bayesian optimization, that is, a global optimization algorithm (Snoek et al., 2012), to efficiently find the best set of parameters. The algorithm iteratively tests different sets of parameter values within the predetermined search space and the set of parameter values leading to the minimum objective function value is designated the optimized values. Simultaneously, the mean relative biomass between diatoms and *Phaeocystis* had to fall within the range of observed values in Figure S3a). The Chl-*a* and phytoplankton relative biomass were chosen for parameter optimization because they can provide good guidance for our model to accurately reproduce both the long-term NPP and the short-term community structure (at limited time scale of the bloom season). Upper and lower parameter bounds for the search space of those parameters were determined from the range of values used previously for the two species (Table 2). Regarding the small species (nanophytoplankton and picophytoplankton), we set a fixed percentage value for diatoms based on the very low contribution of the small species to the total carbon mass in this area (Y. Lee et al., 2016; Yager et al., 2016).

3. Model Implementation, Validation, and Experiment

The 1-D model was used for the western part of the ACS area (Figure 1) from January 1, 1997 to December 31, 2017. We compiled the existing measurement data sets within the model domain for the source of the 1-D initial condition, model relaxation, and parameter optimization and for the assessment of model performance. For the 20 years (1997–2007), the averaged surface Chl-*a* concentrations over the Amundsen Sea shelf area (red tetragon in Figure 1) were determined from the recently reprocessed ocean color data (1 day-binned, 9 km resolution) following the algorithm in Arrigo et al. (2015). NPP integrated over the upper

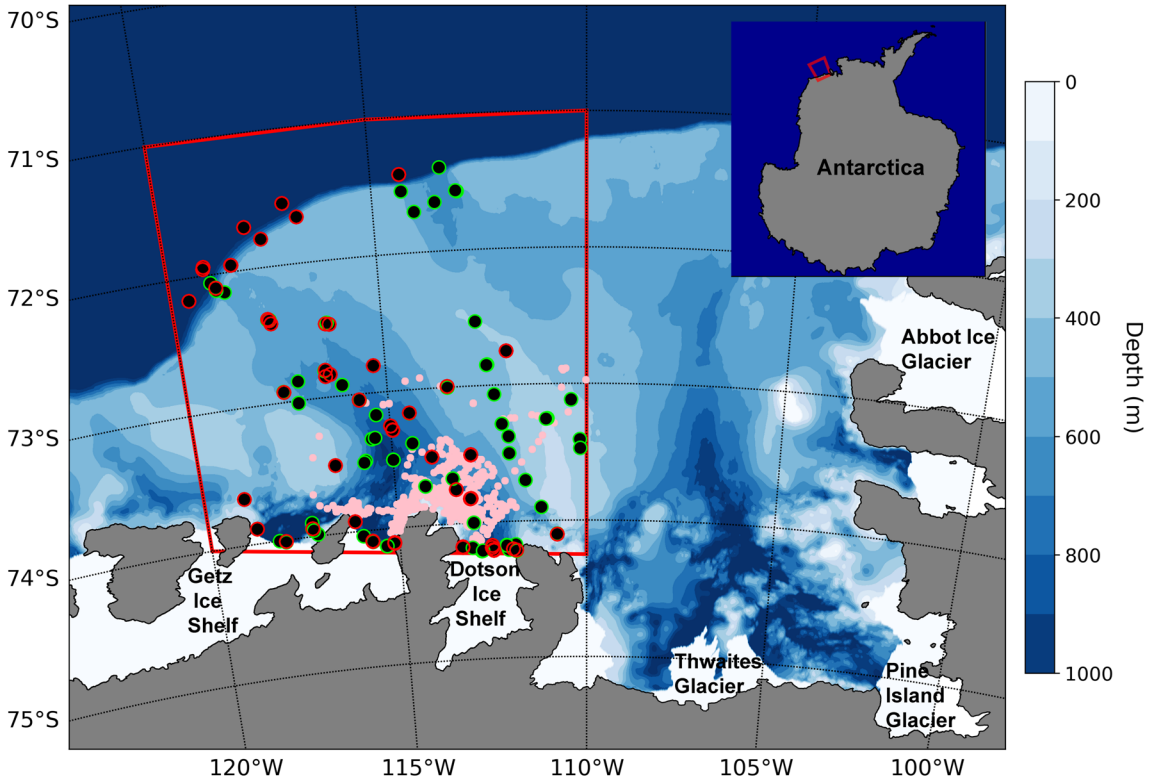

Figure 1. Bathymetry map of the ACS area. Red tetragon denotes the area for which time-series of mean Chl-*a* was obtained and the 1-D model covered. Black dots with lime edge denote the stations of KOPRI cruises where only CTD casting was conducted and the ones with red edge denote the stations where both CTD casting and biogeochemical measurements (Chl-*a*, macronutrients, and in situ NPP) were conducted. The pink dots denote the points where the CTD data were obtained from the MEOP project.

100 m was calculated by the algorithm in Arrigo et al. (2008) using the satellite derived Chl-*a*. CTD data (T/S/Fluorescence) was obtained from the points in Figure 1. Two types of CTD data sets were available. First one encompasses four KOPRI cruises of the IBRV *Araon* from December 2010 to January 2011, from February to March 2012, in January 2014, and from January to February 2016. The other was taken from the Marine mammals Exploring the Oceans Pole to pole (MEOP) project (Treasure et al., 2017) from April to September for only 1 year, 2014. In situ measurements of macronutrients, Chl-*a*, and the water-column integrated NPP were also obtained at the stations of the four KOPRI cruises. The averaged phytoplankton biomass was obtained from two published data sets. One was collected at 12 stations occupied during Amundsen Sea Polynya International Research Expedition (ASPIRE; Yager et al., 2016) from December 14, 2010 to January 5, 2011 that covers the beginning and rise of the bloom. The other was collected at 12 stations within the ACS during a KOPRI cruise for the first 15 days of January 2014 (Y. Lee et al., 2016), the early bloom phase. The averaged profiles of observed iron in polynya area in February 2009 and December 2010 were taken from Gerringa et al. (2012) and Sherrell et al. (2015), respectively. Atmospheric forcing parameters, including zonal and meridional wind speeds, surface air temperature, dew point, and total cloud concentration, were obtained from the 6-hourly ECMWF reanalysis data (ERA-interim; 0.25° horizontal resolution; Dee et al., 2011) as ERA-Interim was reported to be the most reliable reanalysis over Antarctica (Bracegirdle & Marshall, 2012; Bromwich et al., 2011). In order to cover the broad area with the 1-D framework, all field profiles, satellite-derived parameters, and forcing data were averaged over the red tetragon area in Figure 1 for the 1-D array.

The model was run with a 10-min time step and was solved on a vertical domain of the upper 500 m divided into 40 layers. The vertical resolution was the highest (1.6 m) in the surface layer and lowest (21.7 m) in the middle layer. At the lower boundary of the water column, we applied a closed boundary condition. The model was spun-up for 20 years with the atmospheric forcing parameters of 1996 to reach a quasi-equilibrium state. The initial profiles of macronutrients for the spin-up run were taken from the averaged profiles of

the four KOPRI cruises (Figure S4). The initial concentration of dissolved iron for the spin-up run was taken as 0.58 nM uniformly throughout the water column. After the spin-up, the iron concentration below 100 m depth approximated the estimated winter water concentrations, 0.3 nM (Sherrell et al., 2015). The initial conditions for all other state variables were the same as those of Butenschön et al. (2016). The reference simulation analyzed in this study was run for 20 years (1997–2017) after the spin-up run.

For both the spin-up and reference runs, the simple relaxation method for T/S described in Burchard and Petersen (1999) was applied to compensate for the missing hydrodynamic impacts of lateral advections and diffusion and to parameterize the mixed layer depth (MLD) accurately. While the model was relaxed toward the MEOP data for every winter season from April to September, the average profiles of the four KOPRI cruises were used for every summer relaxation (relaxation time scale = 1 day). Following the spin-up, the reference run was initiated, starting in year 1997. It was forced with the forcing parameters of 1997–2017.

We evaluated the reference run results for vertical distributions and surface variations of Chl-*a*, and macronutrients. Three quantitative metrics adopted from Jolliff et al. (2009) were adopted to assess the skill of our model. The RMSE and mean bias error, the measures for the degree of discrepancy between the model and observations, were normalized to the standard deviation of the observation field. The Pearson correlation coefficient (R) is a measure of the degree of linear association between the model and observations.

Using the optimized parameter set, additional model experiments other than the reference run were conducted under variations in the winter concentration of iron and of summer surface irradiance: 0.01–1.0 nM iron before the bloom (August to October) and 10–250 W m^{-2} mid-summer (January) irradiance. We multiplied the surface irradiance by the factors without changing the MLD. These variations reflect the possible increase in iron concentration and surface light availability caused by the increase in glacial meltwater and reductions in ice sheets and sea ice, respectively (Deppeler & Davidson, 2017). The magnitude of the ligand in the current Amundsen Sea (Thuróczy et al., 2012; ~1.1 nM) was considered to be sufficient to cap the iron range we tested here. The resultant biomass values from the different runs were averaged over the growing seasons (November to March) of the 20 years.

4. Results

4.1. Optimized Parameters for the ACS

We obtained the optimal parameters for phytoplankton in the ACS as shown in Table 2. The g_{max} of diatoms is less than 50% of that of *Phaeocystis*, indicating that *Phaeocystis* can grow more rapidly than diatoms if all external limitations on the two species are the same. The lower g_{max} for diatoms is in agreement with the results of previous incubation studies: Strzepek et al. (2011) reported that the g_{max} of one of the predominant diatoms in the Southern Ocean was just 62% of that of *Phaeocystis* under excessive iron conditions, and Arrigo et al. (2010) and Coale et al. (2003) suggested that the g_{max} of diatoms is less than half of that of *Phaeocystis*.

The fact that the k_{Fe} of diatoms is ~8 times lower than that of *Phaeocystis*, however, indicates that diatoms can grow efficiently under the low-iron conditions. According to Coale et al. (2003), it has been reported that the k_{Fe} of *Phaeocystis* is more than twice that of diatoms. Sedwick et al. (2007) also found that the k_{Fe} of *Phaeocystis* can be considerably high (~0.45 nM) in the Ross Sea.

The θ_{max} of diatoms are twice as high as that of *Phaeocystis*, indicating that the Chl-*a*:carbon ratios of diatoms can be twice as high. Given that the ratio of Chl-*a* synthesis to carbon fixation, φ_i, is determined by α and limitation factors as well as by θ_{max} (Equation S6), a higher θ_{max} does not always mean higher efficiency in harvesting light. In addition, the effect of the higher θ_{max} of diatoms can be offset by the prespecified lower value of α for diatoms. Such a considerable difference in Chl-*a* assimilation between diatoms and *Phaeocystis* was also reported by Arrigo et al. (2010), who noted that the cellular Chl-*a*:C ratios of diatoms were ~2.5 times greater than those of *Phaeocystis* at all levels of irradiance.

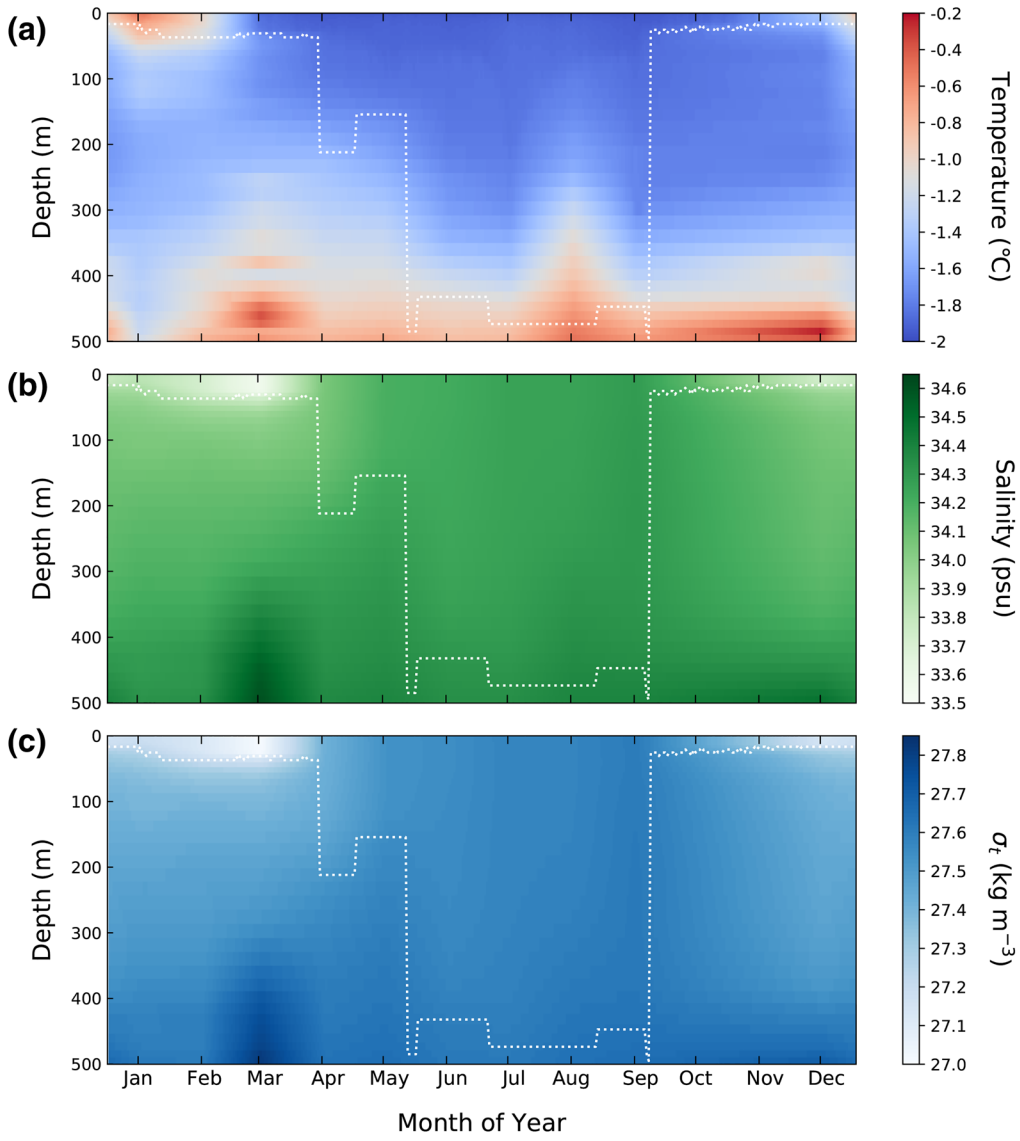

Figure 2. Monthly mean of the model relaxation results for (a) temperature, (b) salinity, and (c) density anomaly (σ_t) from the 20-year reference run. The white dashed line represents the MLD defined at the depth of the maximum of buoyancy frequency (Carvalho et al., 2017).

4.2. Comparison of the Model Simulation and Observations

The resultant physical properties from T/S relaxation are illustrated in Figures 2 and S5. While during the winter season, the MLD developed up to 500 m, it drastically shoaled to ~20 m in the summertime when sea ice melting and sea surface temperature (SST) started to increase. This marked seasonal variation in the MLD leads to a nutrient supply at the surface layers from the deep sea, stimulating phytoplankton blooms in the next spring. We can confirm the relatively saline and warm layer showing the properties of the modified CDW below a depth >300 m. In the uppermost layers, the density stratification by reduced salinity and increased temperature after sea ice melting in the summer season were reflected as well.

Figure 3 displays the time series of the 20-year reference simulation compared with the observations. The simulated surface Chl-*a* used for the parameter optimization agreed well with the observation and NPP was also in reasonable agreement with the observations. The *R* values of the surface Chl-*a* and NPP were 0.80 (p-value < 0.001, df = 7,304) and 0.81 (p-value < 0.001, df = 7,304), respectively (Table S1). Nonetheless, the model slightly underestimated NPP partially due to the different calculations of the model and the

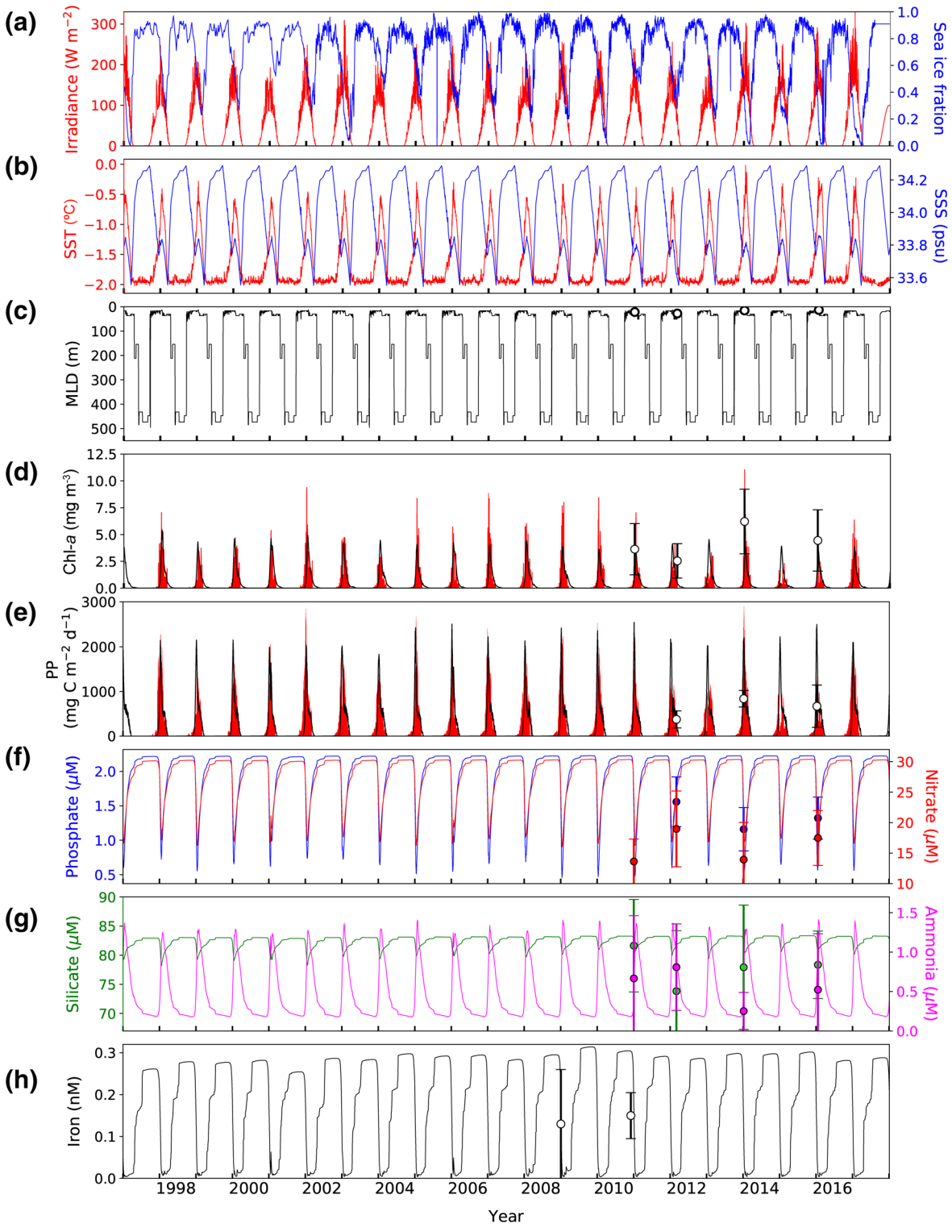

Figure 3. Time series of observations and reference simulations in the surface layer. (a) Simulated irradiance and reanalysis data of the sea ice fraction (ECMWF), (b) simulated SST and SSS, (c) simulated (black line) and observed (open circle) MLD, (d) simulated (black line) and observed (red-shaded range for satellite data and white dots for in situ measurements) surface Chl-*a*, (e) simulated (black line) and observed (red-shaded range for satellite data and white dots for in situ measurements) NPP integrated over the upper 100 m (integrated over the euphotic depth for the in situ value), and (f–h) simulated (solid line) and *in situ* (dots) nutrients. The observed Chl-*a*, NPP, and macronutrients are the averaged values over the all stations (Figure 1) of the individual four KOPRI cruises. The observed iron concentrations near sea surface were taken from Gerringa et al. (2012) and Sherrell et al. (2015).

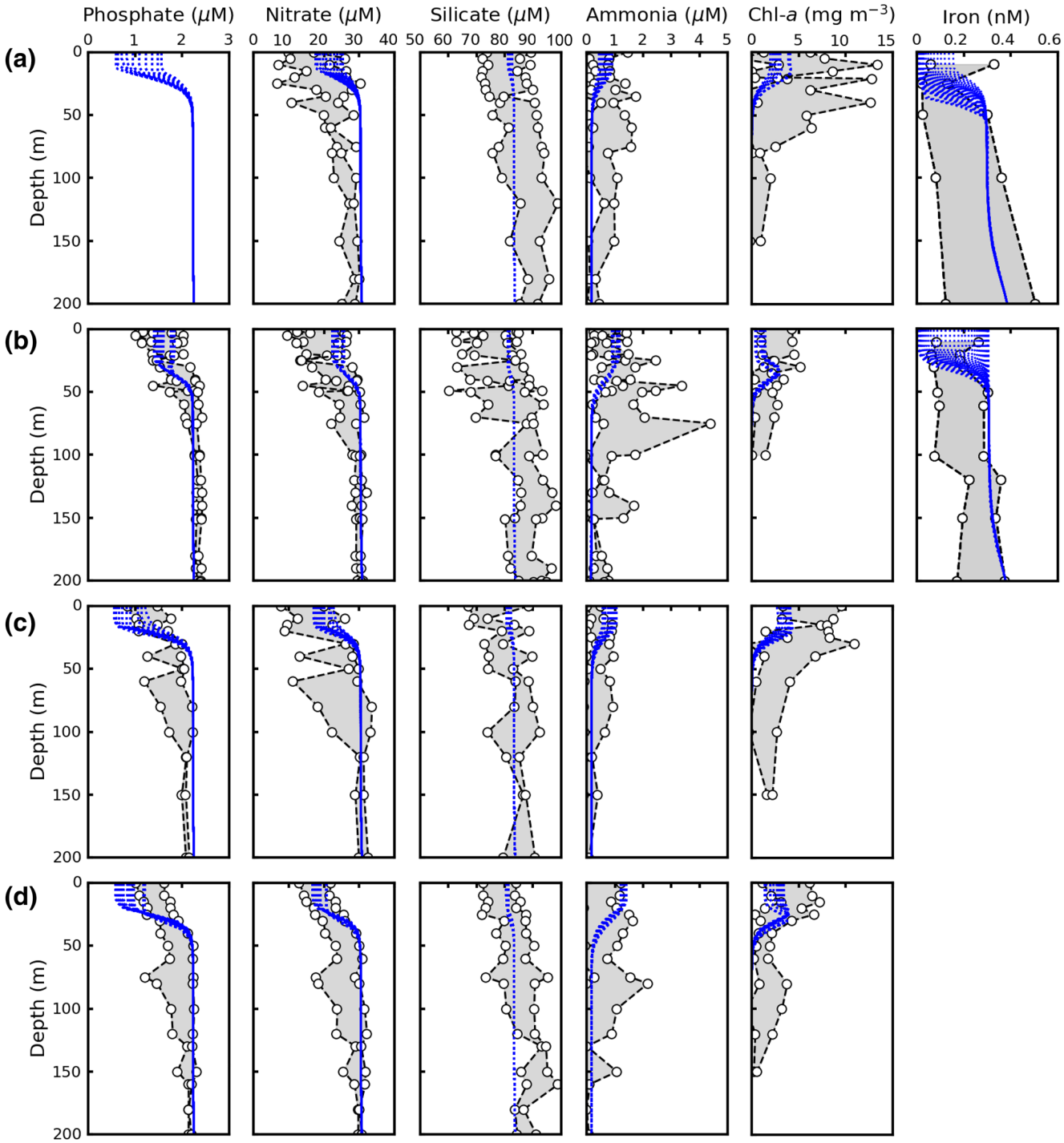

Figure 4. Simulated and observed vertical profiles of macronutrients, Chl-*a*, and dissolved iron for the KOPRI cruise in (a) 2010, (b) 2011/2012, (c) 2014, and (d) 2016. The gray-shaded range indicates the lower and upper limits of the observed data obtained at all stations of the KOPRI cruises. The blue dashed line indicates the model results at the time of sampling. Dissolved iron profiles were digitized from figures of Gerringa et al. (2012) (Stations 113, 114, 119, 142, 148, and 153 in the reference) and Sherrell et al. (2015) (Figure 3e in the reference).

estimation algorithm of satellite NPP. The surface nutrients were in the ranges of in situ measurements in both mid-bloom and late-bloom seasons. The comparisons between simulation and observation of the Wvertical distributions of nutrients and Chl-*a* are displayed in Figure 4. Vertical distributions of biogeochemical variables were generally in the observed ranges and the depth of nutricline was captured by the model.

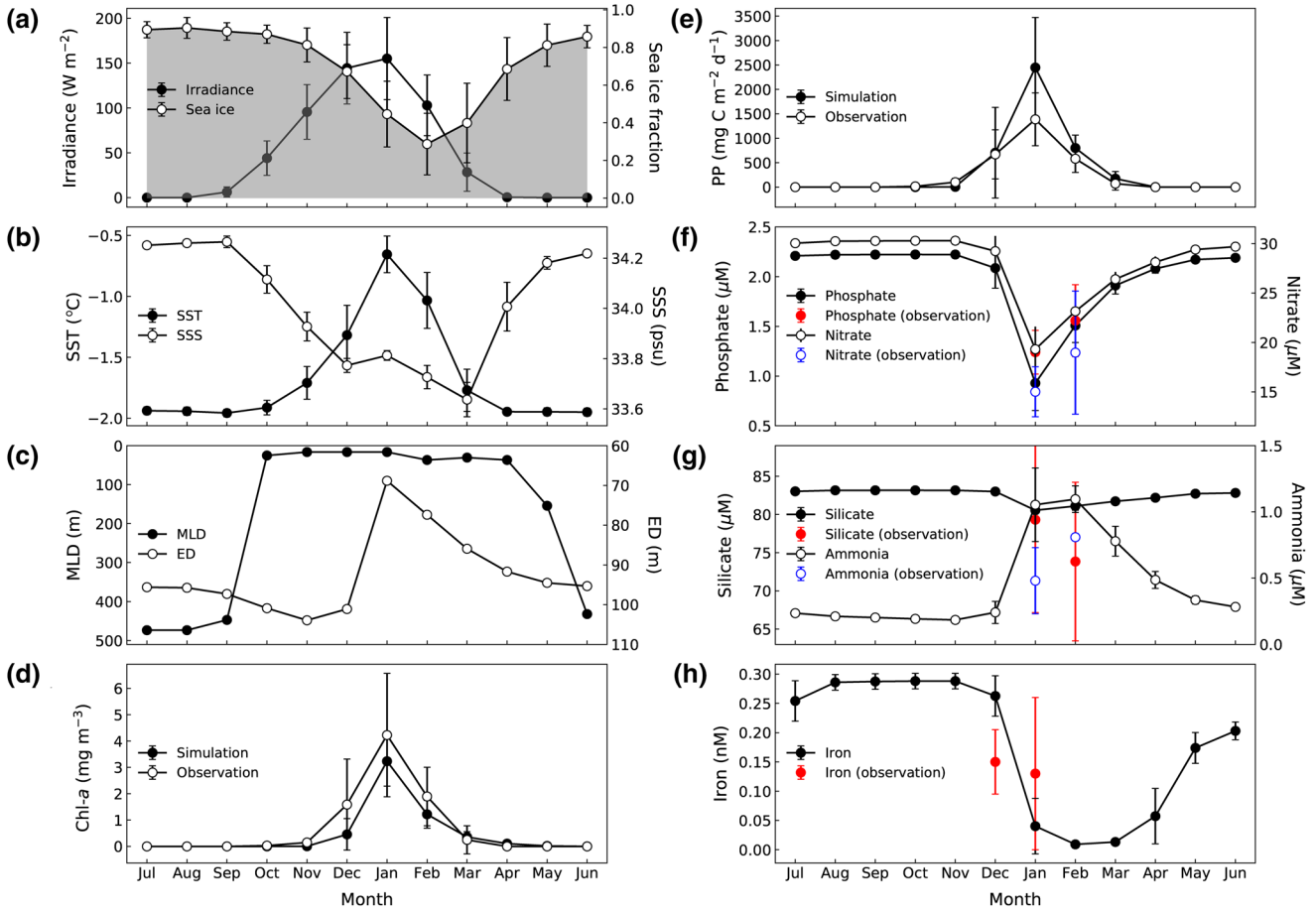

Figure 5. Simulated seasonal variations (monthly mean) of (a) irradiance and sea ice fraction, (b) SST and SSS, (c) MLD and euphotic depth (ED), (d) surface Chl-*a*, (e) NPP integrated over the water column, and (f–h) nutrients. In (a), the sea ice fraction was obtained from ECMWF reanalysis data.

Exceptionally, phosphate near the surface in 2014 and 2016 showed slightly underestimated profiles (Figure 4) while nitrate tended to be biased to the upper limit of the observations. This might stem from 1) the different remineralization rate of phosphorus compared with those of nitrogen and carbon (Yager et al., 2016) and 2) the higher removal ratio of N/P by *Phaeocystis* than diatoms (Arrigo et al., 1999), both of which are not reflected in the current model. Additionally, our model does not represent the different magnitudes of the surface Chl-*a* between years 2014 and 2016, which could be attributable to the absence of the fluctuating lateral advections and other processes that influence the primary production. Our model captured the observed ranges of the surface Chl-*a* and PP, and subsurface nutrients (excluding ammonia and iron) (Figure S6 and Table S1) given that the total RMSE (distance from the origin) values are below 1.0 (Jolliff et al., 2009). Partially due to the lack of observed data compared with other variables, the iron shows a relatively high RMSE value. However, the depleted concentrations near the surface and the winter water layers (>100 m; ~0.3 nM) and the gradual increasing tendency with depth are well reproduced by the model (Figure 4).

4.3. Factors That Shape the Seasonal Phytoplankton Cycle

We illustrated the monthly mean of the 20-year reference run in Figure 5 to investigate the seasonal biogeochemical cycles associated with NPP. The MLD was drastically reduced from October when the retreat of sea ice, the incident light increase, and the SSS reduction started to occur, showing a minimum of ~20 m in December (Figures 5b and 5c). The model showed an approximate ~1 month time lag between the minimal sea ice fraction (February) and the minimal salinity (March) seasons. This could occur because 1) the formation and the retreat of sea ice in this area are strongly influenced by the katabatic wind (Alderkamp et al.,

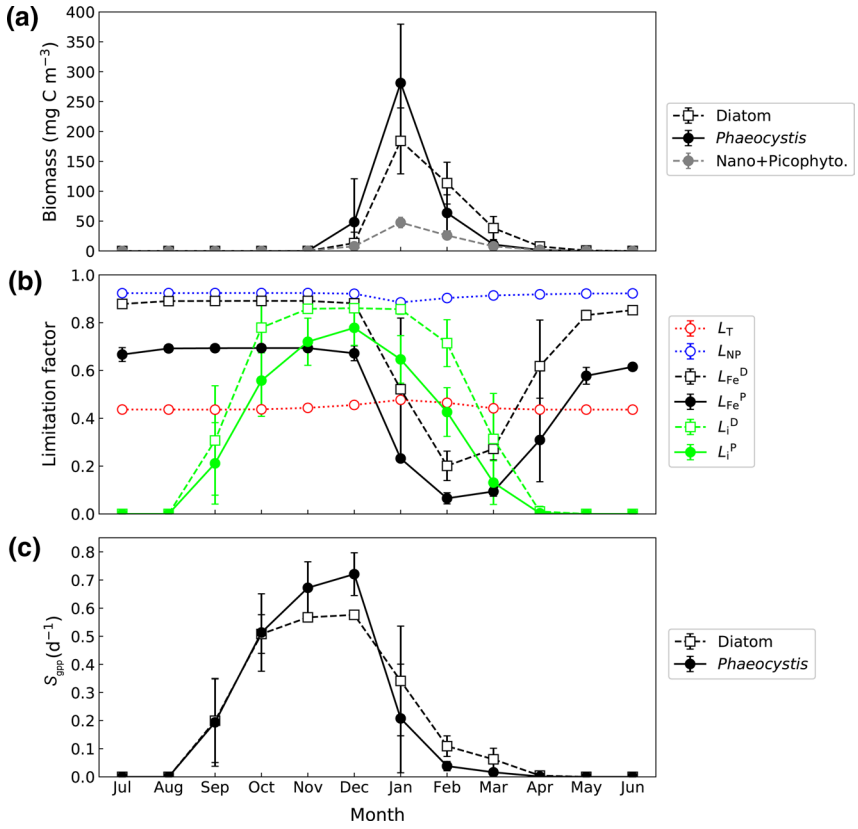

Figure 6. Simulated seasonal variations (monthly mean) of (a) carbon biomass of phytoplankton, (b) limitation factors, and (c) mass-specific growth rates of diatoms and *Phaeocystis*. In (b), the limitation factors of temperature (L_T), nitrate and phosphate (L_{NP}), iron (L_{Fe}; superscript D for diatoms and P for *Phaeocystis*), and irradiance (L_i; superscript D for diatoms and P for *Phaeocystis*) are illustrated. The equations for nutrients and light limitation factors are given in Text S1 (supporting information).

2012b; Arrigo et al., 2012) and 2) the brine convection occurs actively only when some specific environmental requirements are satisfied (Golden et al., 1998, 2007). Although the SSS minimum occurred in March, the MLD deepened from the same month because the SST also decreased with the reduction in irradiance.

The bloom peak, the maximum surface Chl-*a*, occurred in January, showing consistent with observations (Figures 5d and 5e). Without the sea ice effect, the bloom peak appeared in December because of the rapid increase in irradiance (Figure S1). The bloom peak was reduced drastically to its prebloom level by March. Although the surface irradiance remained above 100 W m^{-2} and the macronutrients were replete in February (Figures 5f and 5g), the early termination of the phytoplankton bloom seemed to be mostly attributable to the early depletion of iron at the sea surface (Figure 5h) implying that the iron availability might control the magnitude of phytoplankton biomass and annual NPP of this area.

Figure 6a shows that *Phaeocystis* had a higher biomass (~67% in December and 50% in January) than diatoms (~20% in December and 40% in January) during the early growing season (December) to the peak bloom season (January). After January diatoms showed a higher biomass (~60%) due to more rapid reduction of *Phaeocystis* (~30%). Comparisons of the biomass proportions of the two species from the model and observations for December 2010 and January 2014 are given in Figure S3.

Since phytoplankton biomass mostly depends on the gross primary production (GPP), a product of the mass-specific growth rate and biomass (Text S3 and Figure S7), which is controlled by irradiance, nutrients, and temperature (Equation S2), we investigated the limitation factors for each species in the model (Figure 6b). As macronutrients are generally replete in this area, the L_{NP} and L_s were not reduced considerably even in the summertime (Figures 5f and 5g). The temperature limitation factor (L_T) played a role in reducing the growth rates by approximately half, which is attributed to the low SST (always below zero) for all

seasons. Since the $Q10$ coefficient for all phytoplankton species was 2.0 (Butenschön et al., 2016), L_T was the same for all species. Hence, light or/and iron should play an important role in determining NPP and competition between diatoms and *Phaeocystis*.

The light limitation factor, L_i, began to increase in the early spring (September) when the sea ice retreated and the irradiance started to increase (Figures 5a and 6b). Although *Phaeocystis* has a higher α value than diatoms, it underwent more severe limitation by light (summer mean $L_i = 0.62$, SD = 0.18) than diatoms (summer mean $L_i = 0.81$, SD = 0.08) partially due to the lower θ_{max} of *Phaeocystis* (Table 2). From Equations S4 and S6, we can see that the L_i is influenced by the θ which depends on θ_{max} value.

During the period from November to December when both the biomass and L_i factor were increased, the self-shading effect by phytoplankton in this period is not large enough to reduce L_i and other factors (e.g., increasing incident light) seems to be more important in this period. On the other hand, a slight decreasing pattern for L_i appeared between December and January, resulting in the reductions of L_i from 0.86 to 0.72 for diatoms and from 0.78 to 0.42 for *Phaeocystis*. This implies the phytoplankton biomass in this season is large enough to cause the self-shading effect. Additionally, the lower L_i in January partially resulted from the strong photoinhibition in the period. Nevertheless, L_i remained above 0.4 throughout the summer season (December to February). During the period from January to February, L_{Fe} were nearly half or less than half of L_i for the both species, showing iron is the factor that most decisively limits phytoplankton growth in the summer season, implying that light limitation was not critical for NPP.

Figure 6c shows the mass-specific growth rates (S_{gpp}; see Equation S2) of the two species calculated as g_{max} multiplied by all limitation factors. We confirmed that from November to December, *Phaeocystis* showed a slightly higher S_{gpp} than diatoms. The reason of it despite the lower light and iron limitation factors of *Phaeocystis* is the much higher g_{max} of *Phaeocystis* (Table 2). As a result, the biomass of *Phaeocystis* surpassed that of diatoms during December and January when the phytoplankton biomass reached its maximum. After December, the growth of *Phaeocystis* became lower than that of diatoms because the specific growth rate of *Phaeocystis* decreased more rapidly in this iron-depleted period due to its lower k_{Fe} value (more sensitive to the low iron). This more drastic reduction in S_{gpp} of *Phaeocystis* mainly caused the inversion of the biomass proportion between the two species in February.

4.4. Responses to the Wide Ranges of Iron and Irradiance

By running the model with broad ranges of iron and irradiance scenarios, we found that the threshold for determining the dominant species between the two large species appeared to be ~0.3 nM of iron in the prebloom season (Figure 7a). This threshold concentration tended to increase up to ~0.45 nM as the irradiance decreased. Although the parameters concerning with the light acclimation of the two species were very different as well, the irradiance did not appear to affect the competition between the two species. In addition, both diatoms and *Phaeocystis* showed reductions in their biomass with increasing the irradiance when iron was higher than ~0.2 and ~0.4 nM, respectively. These results stemmed from the nonlinear influence of iron on the L_i value in Equation S4, changing the extents of light limitation and photoinhibition for each species. Total phytoplankton biomass (*Phaeocystis* + diatoms + small species) tended to decrease with increasing iron, while NPP showed the opposite pattern (Figure 7b). Given that diatoms and *Phaeocystis* accounted for most of the phytoplankton biomass (above 90%), the biomass reduction reflects a reduction in the two large species (diatoms and *Phaeocystis*). In addition to the biomass, NPP declined with an irradiance above ~100 W m^{-2} when the iron concentration was higher than ~0.2 nM.

5. Discussion

5.1. Iron Availability Determines the Dominant Species

Iron availability played a critical role in determining the dominant species in the ACS water (Figure 7); the growth rate of diatoms was higher than that of *Phaeocystis* under highly iron-limited conditions, which is ascribed to the low k_{Fe} of diatoms. Indeed, Coale et al. (2003) reported that the inputs of iron to the photic zone can result in dramatic changes in community structure from diatoms-dominated to *Phaeocystis*-dominated system in their deckboard experiments. Although factors controlling the community composition

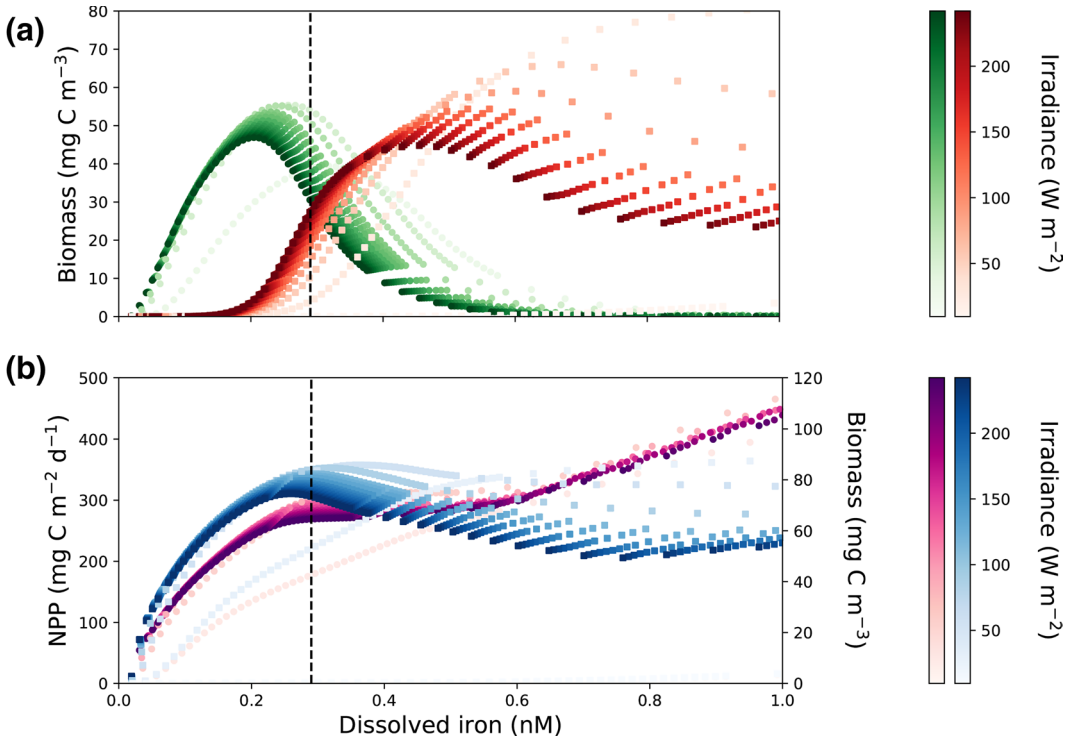

Figure 7. Scatter plots of (a) the biomass of diatoms (green) and *Phaeocystis* (red) and (b) total phytoplankton biomass (blue) and NPP (purple) depending on the iron availabilities from the model experiments under a variety of iron and irradiance conditions. In both (a) and (b), the biomass is averaged within the MLD and NPP is integrated over the MLD. The vertical dashed line denotes the concentration of iron during the prebloom season in the reference simulation.

in the ACS water still remain a subject of intense debate (Arrigo et al., 2003; Boyd et al., 2010; Brussaard et al., 1995; Endo et al., 2017; Feng et al., 2010; Hoppe et al., 2013), several studies have reported that diatoms are better acclimated to low iron concentrations than *Phaeocystis*. For example, using observation- and model-based studies, Strzepek et al. (2011) and Person et al. (2018), respectively, suggested that diatoms tolerate iron-depleted environments by regulating their requirements for cellular iron. From the vertical dashed line in Figure 7, we speculate that even if the iron supply decreases very slightly compared with the present level, there could be a shift in the dominant species toward diatoms, which might impact on the carbon uptake capacity of the ACS.

The recent decreasing trend of sea ice extent can make the pelagic layer to be exposed to the atmosphere and lead to intermittent strong wind-driven mixing (Schultz et al., 2020), which could bring about the reduction in light availability and the increase in nutrients supply into the upper layers. These possible effects should be taken into account to predict how the community structure can be changed in the future. However, given that there have not been any relationships established between the open water duration (data set in Yager et al. [2016]) and MLD, we cannot determine how much the intermittent and transient events of wind-driven mixing can influence the productivity of the whole area of the Amundsen Sea. Given that an increase in meltwater release can also lead to increase in iron and light levels in the upper layers (Arrigo et al., 2015; Duprat et al., 2016; Lin et al., 2011; Moore et al., 2018; Moreau et al., 2015; Vernet et al., 2011), the lower-trophic-level ecosystem could remain dominated by *Phaeocystis* without any large shift in the phytoplankton assemblage.

5.2. Significance of Photoinhibition for the ACS Water Species

Both NPP and total biomass decreased with increasing irradiance when the iron concentration was above ~0.2 nM (Figure 7), likely due to the photoinhibition effect. In Figure 8, we illustrated the combined limitation factor of iron and irradiance (=L_{Fe}× L_i) averaged over the MLD using the mean iron and mean

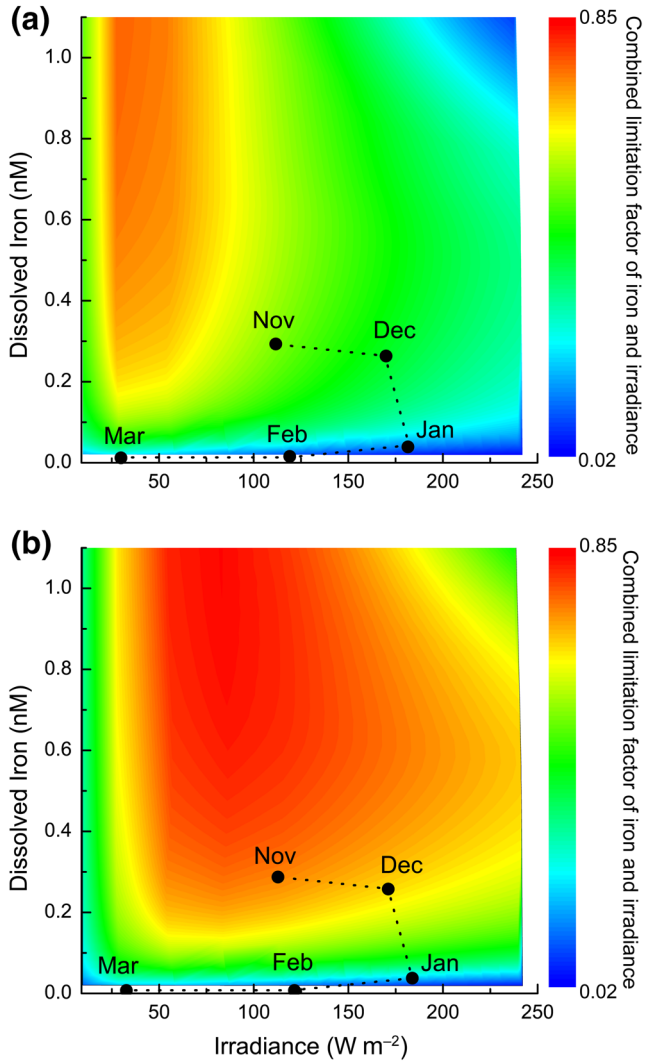

Figure 8. Variations of the combined limitation factor of light and iron averaged over the MLD for (a) diatoms and (b) *Phaeocystis*. Black dots denote the surface iron and irradiance from November to March from the reference simulation.

irradiance from November to March. While the combined limitation factor of diatoms showed the maximum value (optimal growth) at ~50 W m^{-2} irradiance, that of *Phaeocystis* was maximal under ~80 W m^{-2} irradiance. Contrary to studies reporting the better acclimation of *Phaeocystis* to low light than of diatoms (e.g., Alderkamp et al., 2012a), our results indicate that *Phaeocystis* is less susceptible to photoinhibition than diatoms. Joy-Warren et al. (2019) also argue that *Phaeocystis* can adjust to the variable light conditions rather than adjust to the lower light level. Given that the thresholds for photoinhibition of the both species are slightly lower than the current irradiance level in summer (~150 W m^{-2} in January; Figure 5a and black dots in Figure 8), the NPP of the ACS water seems to be inhibited by the too-high irradiance, rather than the limited irradiance, in the upper layer currently. This result conflicts with a general paradigm that the high latitudes are lacking in light for phytoplankton growth. Alderkamp et al. (2010) suggested the potential effect of photoinhibition on the lower-trophic-level biota although their study area (Antarctic Circumpolar Current) is slightly distant from the Antarctic coastal areas. Arrigo et al. (2015) found that the light availability explains little of the variation in NPP over Antarctic polynyas. The incubation experiment by Garcia et al. (2009) implied that *Phaeocystis* in the southern Ross Sea would undergo the photoinhibition effect during the summer.

Our model results suggest that both the iron depletion and the photoinhibition after December lead to termination of phytoplankton bloom. Although Park et al. (2017) and Schofield et al. (2015) suggested the potential significance of light limitation due to the wind-driven mixing, strong mixing in the upper layers is not commonly observed during the summer season and the stratification of the water column in the ACS area is expected to strengthen due to increases in the input of the melt water and warming of surface waters (Deppeler & Davidson, 2017; Moreau et al., 2015).

The argument of Oliver et al. (2019) that self-shading by phytoplankton biomass in the upper ocean during the summer would limit the NPP is also inconsistent with our suggestion. It is noteworthy that our 1-D approach for the overall trend of seasonal and interannual variations in the ACS area does not take into account of the regional variations of light availability due to the changing MLD during the summer season. Additionally, given that the Chl-*a* in the upper layers tended to be overestimated despite the reasonable representations in the whole water column in Oliver et al. (2019), the light limitation could be likely exaggerated than reality. In our model, L_i is governed by nonlinear influences of varying cellular Chl-*a*:C ratio and iron availability as well as α (Equation S4). The intracellular Chl-*a* of *Phaeocystis* should remain lower than that of diatoms under the same conditions due to the lower θ_{max} of *Phaeocystis*, leading to an increase in the photoinhibition index (Equation S2), although the β of *Phaeocystis* is twice as high as that of diatoms. Álvarez et al. (2018) also found that low intracellular Chl-*a* reduced susceptibility to photoinhibition in their modeling study. Our results seem to disagree with some previous studies (e.g., Kropuenske et al., 2010; Mills et al., 2010). However, it is difficult to directly compare these studies to our result because 1) they ignored the interactive effect of iron concentration and 2) still the photosynthetic parameters of *Phaeocystis* are higher than those of diatoms despite the large reduction in the *Phaeocystis* growth rate, indicating that the photosynthesis rate of *Phaeocystis* can surpass that of diatoms. The photoinhibition effect in our model tends to be mitigated as the iron concentration increases, resulting from a positive effect of iron availability on the photoinhibition index (Equation S2). Because of the inherent ability of our model to reflect the relation between iron and photoinhibition, our results are consistent with those of van Oijen et al. (2004) who suggested that iron-limited cells of Antarctic diatoms undergo strong photoinhibition at high irradiance.

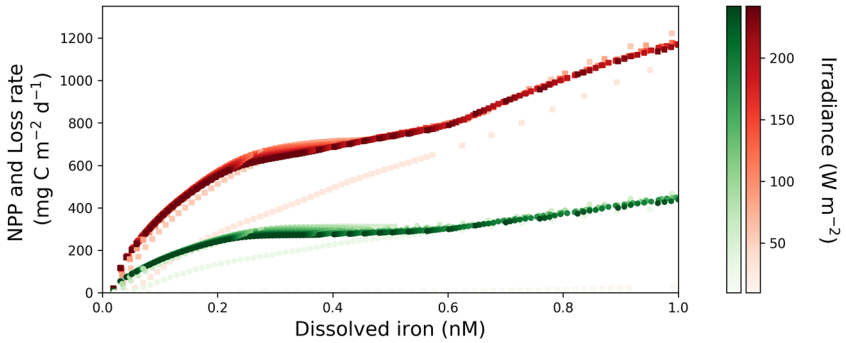

Figure 9. Scatter plot of NPP (greenish) and loss rate (excretion + lysis + grazing; reddish) integrated within the MLD depending on iron availability. The irradiance level is expressed on a color code.

5.3. Meaning of the Inverse Responses of Biomass and NPP to Iron

The opposite responses of NPP and biomass to increasing iron are counterintuitive. However, Moreau et al. (2015) noted that the increase in NPP did not coincide with that of biomass based on long-term trends from satellite-derived observations. In an incubation experiment, Kwon et al. (2015) found that the photosynthetic rate of a diatom species showed an increase while the cellular carbon content was reduced with an increasing iron concentration. Strzepek et al. (2011, 2019) reported that the diatoms can use an adaptive strategy of increasing their cellular ratio of carbon to iron under the depleted iron conditions, showing also that the high carbon mass does not always indicate the high NPP. These results could be explained by larger losses (= excretion + lysis + grazing) of phytoplankton biomass than photosynthesis under high-iron conditions, which means that the sum of the last three terms on the right-hand side of Equation S1 would have a higher increase rate in response to increasing iron concentration than NPP, the sum of the first two terms (= GPP − respiration) (Figure 9). More specifically, even though much of carbon is drawdown by phytoplankton under the iron-replete conditions, it can be excreted as organic forms to balance the cellular element ratios due to the lowered carbon requirements, as it is not assimilated into cellular biomass. Above all, conversion to dissolved organic carbon (DOC) accounted for most of the losses (95%), followed by conversion to POC (3%) and transfer to higher trophic organisms by predation (2%; Figure S8), supporting partially the suggestion by S. Lee et al. (2017). Although our POC flux seems to be extremely low, the comparison with Ducklow et al. (2015) shows that the mean POC flux at a 350 m depth from January 2010 to March 2011 in our model result is comparable to their result (0.72 ± 1.00 in our model vs. 1.38 mmol C m^{-2} d^{-1} in Ducklow et al. [2015]). Given the assumption in ERSEM (Blackford et al., 2004), the large excretion can be interpreted as increase in nutrient-stressed excretion of phytoplankton because of the relatively larger consumptions of nitrate and phosphate with increasing iron availability (Jensen, 1984; Lancelot, 1979) and the consequent reduction in the L_{NP}. Indeed, Figure S9 displays that increasing availabilities of iron lead to a relative reduction in the L_{NP}. Based on this, we suggest that the majority of carbon fixed in the euphotic layer might be converted to the dissolved organic phase by phytoplankton excretion.

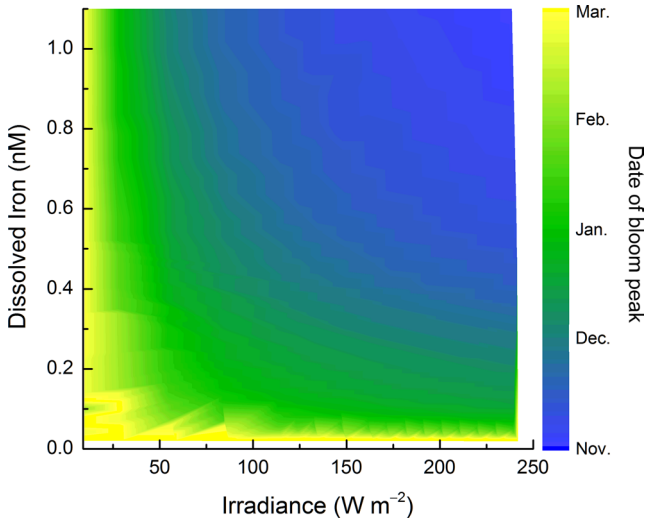

Figure 10. Variation of the month when the total phytoplankton biomass integrated over the MLD reaches its maximum.

The increase in difference between NPP and loss rates with increasing iron and light seems to advance the season of the bloom peak, as shown in Figure 10. The figure shows that the timing when the loss rates surpass NPP was advanced with increasing iron and light. Two reasons potentially explain this. First, stronger top-down processes via the more active loss processes were induced by high iron. Second, bottom-up processes were weakened via advanced photoinhibition by high light. It is notable that the changing conditions of iron and irradiance can impact the seasonal cycles of lower-trophic-level biota as well as the magnitude of NPP.

Simplistically, the photoinhibition can be alleviated with increasing iron due mainly to the increase in glacier meltwater influx. At the same time, increasing DOC release by phytoplankton along with the increasing NPP might raise the carbon fixation in the upper layers and thus the CO_2 uptake during the growing seasons. Furthermore, our model results imply that the DOC release from phytoplankton cells will increase more rapidly than the NPP, which means the majority of fixed carbon in the upper layers is converted into the dissolved phase, not the particulate phase. This suggestion can partially explain the argument of Maiti et al. (2013) that the POC export efficiency in the Southern Ocean has an inverse relationship with the primary production.

5.4. Caveats and Future Studies

Despite its overall good performance, our model still has some limitations. In particular, the interannual variation in NPP could not be reproduced since the ecodynamics in our model depended on only the vertical T/S structure and atmospheric forcing parameters in the absence of the variation in lateral flux of basal melt water and CDW, the large sources of iron (Arrigo et al., 2015; Gerringa et al., 2012; St-Laurent et al., 2017). For example, the observed data showed largely different NPP in 2014 and 2016, although the irradiance levels of the 2 years were similar, which was not captured by the model. Although it is impossible to explicitly simulate the source dynamics with the 1-D water column model, we will be able to consider them by parameterizing the source terms in the specific layers.

We did not consider the transition of *Phaeocystis* including their single cells in small species in this study. It is reported that the main reason for the transition of *Phaeocystis* colonies and single cells is the depletion of nutrients (Garcia et al., 2009; Van Leeuwe & Stefels, 2007). As the small species have low half saturation values for nutrients, we can obtain the result of increased single cells when the nutrients are lowered. Under the conditions of relatively lowered macronutrients (high iron conditions) shown in Figure S9, the small species can increase their growth (up to ~100 mg C m^{-2}; not shown here) because of their lower k_N and k_P than those of the two large species. Moreover, several studies (Marinov et al., 2010; Matebr & Hirst, 1999; Petrou et al., 2016) have suggested that the decline in nutrient supply due to strengthened stratification by future climate change will reduce NPP and favor small flagellate species. It would be necessary to improve our understanding of the small species dynamics as well because they could be another variable affecting future NPP and phytoplankton community compositions. Through field observation near the WAP, Brown et al. (2019) suggested that the community structure between the large diatoms and small cryptophyte species is governed by the meltwater flux from ice sheets and that the CO_2 drawdown can be higher when the large diatom species dominate the system.

Our study presumed that phytoplankton biomass is governed mainly by GPP rather than loss processes such as respiration, lysis, excretion, and grazing. To test this assumption, we investigated the sensitivity of the biomass response to the variation in each term within a range of 20% (Figure S7). Although the biomass was most sensitive to GPP, respiration and cell lysis also appeared to significantly control the biomass. The potential importance of cell lysis has also been reported in other studies (Agusti et al., 2001; Brussaard et al., 1995). Moreover, we confirmed that the loss processes can be elevated as the iron availability increases. Additional experiments are required to understand the potential influences of the loss processes on the biological carbon pump in this area.

In addition, despite a measured cooling over East Antarctica by the year 2000 (Thompson & Solomon, 2002), many studies for the entire Antarctic continental shelf areas predict the similar future trends such as an increase in the SST and iron availability, with decreases in the MLD and ice sheets concentration (Moore et al., 2018; Rickard & Behrens, 2016). Our model suggestion that the biological pump through NPP would increase with increasing iron concentration in the future might be applicable to the entire ACS regions. However, the parameters that determine the physiological properties of both diatoms and *Phaeocystis* are known to show the spatial and temporal variations depending on their habitat environments (Cavan et al., 2019; Garcia et al., 2009; Hutchins & Boyd, 2016; Kropuenske et al., 2009), making the generalization premature. Consistent researches is required in order to accurately predict the possible variations in the Amundsen Sea productivity as there are some missing factors although our model results indicate that the increasing iron concentration in the near future would increase the NPP. Future studies should be focused on 1) the residence time of DOC fixed in the euphotic layer by investigating the microbial activities, 2)

the pathways and outgassing rate of the introduced dissolved inorganic carbon (DIC) from the upwelled CDW-originated waters through the vertical mixing and the advection, and 3) the quantitative assessment of iron organic-ligands flux and dynamics. Although we expect that the NPP of the Amundsen Sea would increase in the future, the remineralization time scale of the fixed carbon and the outgassing of the high DIC in the CDW-derived waters are the ultimate controllers of the carbon uptake capacity of this region. We also need to understand the dynamics of organic ligands that keep the iron in bioavailable to complement our suggestions on the increase in NPP and the strengthening of the *Phaeocystis*-dominant ecosystem over the ACS region with future increases in glacier-derived iron (Gerringa et al., 2012; Thuróczy et al., 2012).

6. Summary and Conclusions

We investigated the influences of iron and light availabilities on NPP and phytoplankton competition using a 1-D marine ecosystem model enhanced by incorporating sea ice effects and optimizing the parameters for diatoms and *Phaeocystis*, the two dominant species in the ACS water. According to our model results, the irradiance during the summer season was sufficient or excessive for the bloom of phytoplankton and rapid depletion of iron appeared to be the main reason for the early termination of bloom before sea ice recovery. Additionally, the iron availability played a role in determining the dominant species as well as the magnitude of NPP. Diatoms can be dominant under low-iron conditions, while *Phaeocystis* can dominate the community under the relatively iron-replete conditions. With increasing iron availability, conversion of carbon to nonliving organic pool by phytoplankton exudation increased much more rapidly than NPP, implying a reduction in the carbon biomass. It implies that the negative feedback of the ACS water to the global warming trend would increase given that the iron limitation can be alleviated by the increase in influx of glacier meltwater. It is noteworthy that increases in iron and irradiance can also lead to a shift in the bloom peak timing to earlier than January due to increasing loss processes and photoinhibition. Our model results confirmed that phytoplankton responses to environmental changes were driven by both individual and interactive stressors. The nonlinear relations of NPP and phytoplankton biomass with variations in iron and irradiance suggest that accurately predicting ecosystem responses to future climatic changes will be a complex challenge. Our understanding should be increased through the quantitative investigations of the interactions of multiple stressors for the primary production and the iron dynamics so that we comprehend and predict accurately carbon uptake capacity of the entire ACS waters.

Data Availability Statement

ERSEM and GOTM source codes are available at https://pml.ac.uk/Modelling_at_PML/Access_Code and https://gotm.net/portfolio/software/, respectively. ECMWF ERA-Interim reanalysis data are available at https://www.ecmwf.int/en/forecasts/datasets/reanalysis-datasets/era-interim. The phytoplankton carbon biomass and iron data sets are included in these papers: Y. Lee et al. (2016), Yager et al. (2016), and Sherrell et al. (2015). The remote sensing data sets, CTD, NPP, Chl-*a*, macronutrients and reference run output file are from https://datadryad.org/.

Acknowledgments
This work was supported by the Korea Polar Research Institute program (PE21110), the National Research Foundation of Korea (NRF) grant funded by the Korea government (MSIT) (No. NRF-2018H1A2A1060886), and the Ministry of Oceans and Fisheries (20170336). We would also like to thank Kevin R. Arrigo for sharing his remote sensing data.

References

Agusti, S., Duarte, C. M., Vaqué, D., Hein, M., Gasol, J. M., & Vidal, M. (2001). Food-web structure and elemental (C, N and P) fluxes in the eastern tropical North Atlantic. *Deep Sea Research Part II: Topical Studies in Oceanography*, *48*(10), 2295–2321.

Alderkamp, A. C., de Baar, H. J., Visser, R. J., & Arrigo, K. R. (2010). Can photoinhibition control phytoplankton abundance in deeply mixed water columns of the Southern Ocean? *Limnology and Oceanography*, *55*(3), 1248–1264.

Alderkamp, A. C., Kulk, G., Buma, A. G., Visser, R. J., Van Dijken, G. L., Mills, M. M., & Arrigo, K. R. (2012a). The effect of iron limitation on the photophysiology of *Phaeocystis antarctica* (Prymnesiophyceae) and *Fragilariopsis cylindrus* (Bacillariophyceae) under dynamic irradiance. *Journal of Phycology*, *48*(1), 45–59. https://doi.org/10.1111/j.1529-8817.2011.01098.x

Alderkamp, A. C., Mills, M. M., van Dijken, G. L., Laan, P., Thuroczy, C. E., Gerringa, L. J. A., et al. (2012b). Iron from melting glaciers fuels phytoplankton blooms in the Amundsen Sea (Southern Ocean): Phytoplankton characteristics and productivity. *Deep-Sea Research Part II-Topical Studies in Oceanography*, *71–76*, 32–48. https://doi.org/10.1016/j.dsr2.2012.03.005

Alderkamp, A. C., van Dijken, G. L., Lowry, K. E., Connelly, T. L., Lagerstrom, M., Sherrell, R. M., et al. (2015). Fe availability drives phytoplankton photosynthesis rates during spring bloom in the Amundsen Sea Polynya, Antarctica. *Elementa-Science of the Anthropocene*, *3*, 000043. https://doi.org/10.12952/journal.elementa.000043

Allen, J. I., Siddorn, J. R., Blackford, J. C., & Gilbert, F. J. (2004). Turbulence as a control on the microbial loop in a temperate seasonally stratified marine systems model. *Journal of Sea Research*, *52*(1), 1–20. https://doi.org/10.1016/j.seares.2003.09.004

Allison, I., Brandt, R. E., & Warren, S. G. (1993). East Antarctic sea ice – Albedo, thickness distribution, and snow cover. *Journal of Geophysical Research*, *98*(C7), 12417–12429. https://doi.org/10.1029/93jc00648

Álvarez, E., Thoms, S., & Völker, C. (2018). Chlorophyll to carbon ratio derived from a global ecosystem model with photodamage. *Global Biogeochemical Cycles*, *32*(5), 799–816. https://doi.org/10.1029/2017gb005850

Annett, A. L., Carson, D. S., Crosta, X., Clarke, A., & Ganeshram, R. S. (2010). Seasonal progression of diatom assemblages in surface waters of Ryder Bay, Antarctica. *Polar Biology*, *33*(1), 13–29.

Arrigo, K. R., DiTullio, G. R., Dunbar, R. B., Robinson, D. H., VanWoert, M., Worthen, D. L., & Lizotte, M. P. (2000). Phytoplankton taxonomic variability in nutrient utilization and primary production in the Ross Sea. *Journal of Geophysical Research*, *105*(C4), 8827–8846. https://doi.org/10.1029/1998jc000289

Arrigo, K. R., Lowry, K. E., & van Dijken, G. L. (2012). Annual changes in sea ice and phytoplankton in polynyas of the Amundsen Sea, Antarctica. *Deep-Sea Research Part II-Topical Studies in Oceanography*, *71–76*, 5–15. https://doi.org/10.1016/j.dsr2.2012.03.006

Arrigo, K. R., Mills, M. M., Kropuenske, L. R., van Dijken, G. L., Alderkamp, A. C., & Robinson, D. H. (2010). Photophysiology in two major Southern Ocean phytoplankton taxa: Photosynthesis and growth of *Phaeocystis antarctica* and *Fragilariopsis cylindrus* under different irradiance levels. *Integrative and Comparative Biology*, *50*(6), 950–966. https://doi.org/10.1093/icb/icq021

Arrigo, K. R., Robinson, D. H., Worthen, D. L., Dunbar, R. B., DiTullio, G. R., VanWoert, M., & Lizotte, M. P. (1999). Phytoplankton community structure and the drawdown of nutrients and CO_2 in the Southern Ocean. *Science*, *283*(5400), 365–367. https://doi.org/10.1126/science.283.5400.365

Arrigo, K. R., & van Dijken, G. L. (2003). Phytoplankton dynamics within 37 Antarctic coastal polynya systems. *Journal of Geophysical Research*, *108*, 3271. https://doi.org/10.1029/2002jc001739

Arrigo, K. R., van Dijken, G. L., & Bushinsky, S. (2008). Primary production in the Southern Ocean, 1997–2006. *Journal of Geophysical Research*, *113*, C08004. https://doi.org/10.1029/2007jc004551

Arrigo, K. R., van Dijken, G. L., & Strong, A. L. (2015). Environmental controls of marine productivity hot spots around Antarctica. *Journal of Geophysical Research: Oceans*, *120*(8), 5545–5565. https://doi.org/10.1002/2015jc010888

Arrigo, K. R., Worthen, D. L., & Robinson, D. H. (2003). A coupled ocean-ecosystem model of the Ross Sea: 2. Iron regulation of phytoplankton taxonomic variability and primary production. *Journal of Geophysical Research*, *108*, 3231. https://doi.org/10.1029/2001jc000856

Asper, V. L., & Smith, W. O. (1999). Particle fluxes during austral spring and summer in the southern Ross Sea, Antarctica. *Journal of Geophysical Research*, *104*(C3), 5345–5359. https://doi.org/10.1029/1998jc900067

Aumont, O., Maier-Reimer, E., Blain, S., & Monfray, P. (2003). An ecosystem model of the global ocean including Fe, Si, P colimitations. *Global Biogeochemical Cycles*, *17*, 1060. https://doi.org/10.1029/2001gb001745

Blackford, J. C., Allen, J. I., & Gilbert, F. J. (2004). Ecosystem dynamics at six contrasting sites: a generic modelling study. *Journal of Marine Systems*, *52*(1-4), 191–215. https://doi.org/10.1016/j.jmarsys.2004.02.004

Boyd, P. W., & Brown, C. J. (2015). Modes of interactions between environmental drivers and marine biota. *Frontiers in Marine Science*, *2*(9), 1–7. https://doi.org/10.3389/fmars.2015.00009

Boyd, P. W., Dillingham, P. W., McGraw, C. M., Armstrong, E. A., Cornwall, C. E., Feng, Y. Y., et al. (2016). Physiological responses of a Southern Ocean diatom to complex future ocean conditions. *Nature Climate Change*, *6*(2), 207–213. https://doi.org/10.1038/nclimate2811

Boyd, P. W., Strzepek, R., Fu, F., & Hutchins, D. A. (2010). Environmental control of open-ocean phytoplankton groups: Now and in the future. *Limnology and Oceanography*, *55*(3), 1353–1376. https://doi.org/10.4319/lo.2010.55.3.1353

Bracegirdle, T. J., & Marshall, G. J. (2012). The reliability of Antarctic tropospheric pressure and temperature in the latest global reanalyses. *Journal of Climate*, *25*(20), 7138–7146.

Bromwich, D. H., Nicolas, J. P., & Monaghan, A. J. (2011). An assessment of precipitation changes over Antarctica and the Southern Ocean since 1989 in contemporary global reanalyses. *Journal of Climate*, *24*(16), 4189–4209.

Brown, M. S., Munro, D. R., Feehan, C. J., Sweeney, C., Ducklow, H. W., & Schofield, O. M. (2019). Enhanced oceanic CO_2 uptake along the rapidly changing West Antarctic Peninsula. *Nature Climate Change*, *9*(9), 678–683.

Brussaard, C., Riegman, R., Noordeloos, A., Cadée, G., Witte, H., Kop, A., et al. (1995). Effects of grazing, sedimentation and phytoplankton cell lysis on the structure of a coastal pelagic food web. *Marine Ecology Progress Series*, *123*, 259–271.

Burchard, H., & Petersen, O. (1999). Models of turbulence in the marine environment – A comparative study of two-equation turbulence models. *Journal of Marine Systems*, *21*(1–4), 29–53. https://doi.org/10.1016/S0924-7963(99)00004-4

Butenschön, M., Clark, J., Aldridge, J. N., Allen, J. I., Artioli, Y., Blackford, J., et al. (2016). ERSEM 15.06: A generic model for marine biogeochemistry and the ecosystem dynamics of the lower trophic levels. *Geoscientific Model Development*, *9*(4), 1293–1339. https://doi.org/10.5194/gmd-9-1293-2016

Carvalho, F., Kohut, J., Oliver, M. J., & Schofield, O. (2017). Defining the ecologically relevant mixed-layer depth for Antarctica's coastal seas. *Geophysical Research Letters*, *44*(1), 338–345. https://doi.org/10.1002/2016gl071205

Cavan, E. L., Henson, S. A., & Boyd, P. W. (2019). The sensitivity of subsurface microbes to ocean warming accentuates future declines in particulate carbon export. *Frontiers in Ecology and Evolution*, *6*, 1–10. https://doi.org/10.3389/fevo.2018.00230

Coale, K. H., Wang, X., Tanner, S. J., & Johnson, K. S. (2003). Phytoplankton growth and biological response to iron and zinc addition in the Ross Sea and Antarctic Circumpolar Current along 170°W. *Deep Sea Research Part II: Topical Studies in Oceanography*, *50*(3), 635–653. https://doi.org/10.1016/S0967-0645(02)00588-X

Davidson, A. T., & Marchant, H. J. (1992). Protist abundance and carbon concentration during a Phaeocystis-dominated bloom at an Antarctic coastal site. *Polar Biology*, *12*(3–4), 387–395.

Deb, P., Orr, A., Bromwich, D. H., Nicolas, J. P., Turner, J., & Hosking, J. S. (2018). Summer drivers of atmospheric variability affecting ice shelf thinning in the Amundsen Sea Embayment, West Antarctica. *Geophysical Research Letters*, *45*(9), 4124–4133. https://doi.org/10.1029/2018gl077092

Dee, D. P., Uppala, S. M., Simmons, A. J., Berrisford, P., Poli, P., Kobayashi, S., et al. (2011). The ERA-Interim reanalysis: Configuration and performance of the data assimilation system. *Quarterly Journal of the Royal Meteorological Society*, *137*(656), 553–597. https://doi.org/10.1002/qj.828

Delmont, T. O., Hammar, K. M., Ducklow, H. W., Yager, P. L., & Post, A. F. (2014). *Phaeocystis antarctica* blooms strongly influence bacterial community structures in the Amundsen Sea polynya. *Frontiers in Microbiology*, *5*, 646. https://doi.org/10.3389/fmicb.2014.00646

Deppeler, S. L., & Davidson, A. T. (2017). Southern Ocean phytoplankton in a changing climate. *Frontiers in Marine Science*, *4*, 1–28. https://doi.org/10.3389/fmars.2017.00040

DiTullio, G., Grebmeier, J., Arrigo, K., Lizotte, M., Robinson, D., Leventer, A., et al. (2000). Rapid and early export of *Phaeocystis antarctica* blooms in the Ross Sea, Antarctica. *Nature*, *404*(6778), 595.

DiTullio, G. R., & Smith, W. O. (1996). Spatial patterns in phytoplankton biomass and pigment distributions in the Ross Sea. *Journal of Geophysical Research*, *101*(C8), 18467–18477.
Doucette, G. J., & Harrison, P. J. (1990). Some effects of iron and nitrogen stress on the red tide dinoflagellate Gymnodinium-sanguineum. *Marine Ecology Progress Series*, *62*(3), 293–306. https://doi.org/10.3354/meps062293
Ducklow, H. W., Wilson, S. E., Post, A. F., Stammerjohn, S. E., Erickson, M., Lee, S., et al. (2015). Particle flux on the continental shelf in the Amundsen Sea Polynya and Western Antarctic Peninsula. *Elementa-Science of the Anthropocene*, *3*, 000046. https://doi.org/10.12952/journal.elementa.000046
Duprat, L. P. A. M., Bigg, G. R., & Wilton, D. J. (2016). Enhanced Southern Ocean marine productivity due to fertilization by giant icebergs. *Nature Geoscience*, *9*(3), 219–221. https://doi.org/10.1038/ngeo2633
Endo, H., Hattori, H., Mishima, T., Hashida, G., Sasaki, H., Nishioka, J., & Suzuki, K. (2017). Phytoplankton community responses to iron and CO_2 enrichment in different biogeochemical regions of the Southern Ocean. *Polar Biology*, *40*(11), 2143–2159.
Feng, Y., Hare, C. E., Rose, J. M., Handy, S. M., DiTullio, G. R., Lee, P. A., et al. (2010). Interactive effects of iron, irradiance and CO_2 on Ross Sea phytoplankton. *Deep-Sea Research Part I-Oceanographic Research Papers*, *57*(3), 368–383. https://doi.org/10.1016/j.dsr.2009.10.013
Frölicher, T. L., Sarmiento, J. L., Paynter, D. J., Dunne, J. P., Krasting, J. P., & Winton, M. (2015). Dominance of the Southern Ocean in anthropogenic carbon and heat uptake in CMIP5 models. *Journal of Climate*, *28*(2), 862–886. https://doi.org/10.1175/jcli-d-14-00117.1
Garcia, N. S., Sedwick, P. N., & DiTullio, G. R. (2009). Influence of irradiance and iron on the growth of colonial *Phaeocystis antarctica*: Implications for seasonal bloom dynamics in the Ross Sea, Antarctica. *Aquatic Microbial Ecology*, *57*, 203–220. https://doi.org/10.3354/ame01334
Garibotti, I. A., Vernet, M., & Ferrario, M. E. (2005). Annually recurrent phytoplanktonic assemblages during summer in the seasonal ice zone west of the Antarctic Peninsula (Southern Ocean). *Deep Sea Research Part I: Oceanographic Research Papers*, *52*(10), 1823–1841.
Geider, R. J., La Roche, J., Greene, R. M., & Olaizola, M. (1993). Response of the photosynthetic apparatus of *Phaeodactylum tricornutum* (Bacillariophyceae) to nitrate, phosphate, or iron starvation. *Journal of Phycology*, *29*(6), 755–766.
Geider, R. J., MacIntyre, H. L., & Kana, T. M. (1998). A dynamic regulatory model of phytoplanktonic acclimation to light, nutrients, and temperature. *Limnology and Oceanography*, *43*(4), 679–694. https://doi.org/10.4319/lo.1998.43.4.0679
Gerringa, L. J. A., Alderkamp, A. C., Laan, P., Thuróczy, C. E., De Baar, H. J. W., Mills, M. M., et al. (2012). Iron from melting glaciers fuels the phytoplankton blooms in Amundsen Sea (Southern Ocean): Iron biogeochemistry. *Deep-Sea Research Part II-Topical Studies in Oceanography*, *71–76*, 16–31. https://doi.org/10.1016/j.dsr2.2012.03.007
Golden, K., Ackley, S., & Lytle, V. (1998). The percolation phase transition in sea ice. *Science*, *282*(5397), 2238–2241.
Golden, K., Eicken, H., Heaton, A. L., Miner, J., Pringle, D. J., & Zhu, J. (2007). Thermal evolution of permeability and microstructure in sea ice. *Geophysical Research Letters*, *34*, L16501. https://doi.org/10.1029/2007GL030447
Hoffmann, L. J., Peeken, I., Lochte, K., Assmy, P., & Veldhuis, M. (2006). Different reactions of Southern Ocean phytoplankton size classes to iron fertilization. *Limnology and Oceanography*, *51*(3), 1217–1229. https://doi.org/10.4319/lo.2006.51.3.1217
Hood, E. M., Merlivat, L., & Johannessen, T. (1999). Variations of fCO_2 and air-sea flux of CO_2 in the Greenland Sea gyre using high-frequency time series data from CARIOCA drift buoys. *Journal of Geophysical Research*, *104*(C9), 20571–20583. https://doi.org/10.1029/1999jc900130
Hoppe, C. J., Hassler, C. S., Payne, C. D., Tortell, P. D., Rost, B., & Trimborn, S. (2013). Iron limitation modulates ocean acidification effects on southern ocean phytoplankton communities. *PLoS One*, *8*(11), e79890. https://doi.org/10.1371/journal.pone.0079890
Hutchins, D. A., & Boyd, P. W. (2016). Marine phytoplankton and the changing ocean iron cycle. *Nature Climate Change*, *6*(12), 1072–1079. https://doi.org/10.1038/nclimate3147
Jabre, L., & Bertrand, E. M. (2020). Interactive effects of iron and temperature on the growth of *Fragilariopsis cylindrus*. *Limnology and Oceanography Letters*, *5*, 363–370. https://doi.org/10.1002/lol2.10158
Jensen, A. (1984). Excretion of organic carbon as function of nutrient stress. In O. Holm-Hansen, L. Bolis, & R. Gilles (Eds.), *Marine Phytoplankton and Productivity: Proceedings of the invited lectures to a symposium organized within the 5th conference of the European Society for Comparative Physiology and Biochemistry — Taormina, Sicily, Italy, September 5–8, 1983* (pp. 61–72). Berlin, Heidelberg: Springer Berlin Heidelberg. https://doi.org/10.1007/978-3-662-02401-0_6
Jolliff, J. K., Kindle, J. C., Shulman, I., Penta, B., Friedrichs, M. A. M., Helber, R., & Arnone, R. A. (2009). Summary diagrams for coupled hydrodynamic-ecosystem model skill assessment. *Journal of Marine Systems*, *76*(1–2), 64–82. https://doi.org/10.1016/j.jmarsys.2008.05.014
Joy-Warren, H. L., van Dijken, G. L., Alderkamp, A. -C., Leventer, A., Lewis, K. M., & Selz, V. (2019). Light Is the Primary Driver of Early Season Phytoplankton Production Along the Western Antarctic Peninsula. *Journal of Geophysical Research: Oceans*, *124*(11), 7375–7399. https://doi.org/10.1029/2019jc015295
Khatiwala, S., Primeau, F., & Hall, T. (2009). Reconstruction of the history of anthropogenic CO_2 concentrations in the ocean. *Nature*, *462*(7271), 346–349. https://doi.org/10.1038/nature08526
Kropuenske, L. R., Mills, M. M., Van Dijken, G. L., Alderkamp, A. C., Mine Berg, G., Robinson, D. H., et al. (2010). Strategies and rates of photoacclimation in two major Southern Ocean phytoplankton taxa: *Phaeocystis antarctica* (Haptophyta) and *Fragilariopsis cylindrus* (Bacillariophyceae). *Journal of Phycology*, *46*(6), 1138–1151.
Kropuenske, L. R., Mills, M. M., van Dijken, G. L., Bailey, S., Robinson, D. H., Welschmeyer, N. A., & Arrigo, K. R. (2009). Photophysiology in two major Southern Ocean phytoplankton taxa: Photoprotection in *Phaeocystis antarctica* and *Fragilariopsis cylindrus*. *Limnology and Oceanography*, *54*(4), 1176–1196. https://doi.org/10.4319/lo.2009.54.4.1176
Kwon, Y. S., Rhee, T. S., Kim, S. Y., Kim, M. S., Choi, M. S., Yang, E. J., & Kim, Y.-N. (2015). *Fragilariopsis kerguelensis* response to iron enrichment regarding its growth, uptake of nutrients and trace metals, and changes in CO_2, CH_4, and N_2O. *Ocean Science Journal*, *49*(4), 449–463. https://doi.org/10.1007/s12601-014-0042-5
Lancelot, C. (1979). Gross excretion rates of natural marine phytoplankton and heterotrophic uptake of excreted products in the southern North Sea, as determined by short-term kinetics. *Marine Ecology Progress Series*, *1*, 179–186.
Lancelot, C., Spitz, Y., Gypens, N., Ruddick, K., Becquevort, S., Rousseau, V., et al. (2005). Modelling diatom and Phaeocystis blooms and nutrient cycles in the Southern Bight of the North Sea: The MIRO model. *Marine Ecology Progress Series*, *289*, 63–78. https://doi.org/10.3354/meps289063
Lee, S., Hwang, J., Ducklow, H. W., Hahm, D., Lee, S. H., Kim, D., et al. (2017). Evidence of minimal carbon sequestration in the productive Amundsen Sea polynya. *Geophysical Research Letters*, *44*(15), 7892–7899. https://doi.org/10.1002/2017gl074646
Lee, Y., Yang, E. J., Park, J., Jung, J., Kim, T. W., & Lee, S. (2016). Physical-biological coupling in the Amundsen Sea, Antarctica: Influence of physical factors on phytoplankton community structure and biomass. *Deep Sea Research Part I: Oceanographic Research Papers*, *117*, 51–60. https://doi.org/10.1016/j.dsr.2016.10.001

Lin, H., Rauschenberg, S., Hexel, C. R., Shaw, T. J., & Twining, B. S. (2011). Free-drifting icebergs as sources of iron to the Weddell Sea. *Deep Sea Research Part II: Topical Studies in Oceanography*, *58*(11–12), 1392–1406. https://doi.org/10.1016/j.dsr2.2010.11.020

Maiti, K., Charette, M. A., Buesseler, K. O., & Kahru, M. (2013). An inverse relationship between production and export efficiency in the Southern Ocean. *Geophysical Research Letters*, *40*(8), 1557–1561. https://doi.org/10.1002/grl.50219

Marinov, I., Doney, S. C., & Lima, I. D. (2010). Response of ocean phytoplankton community structure to climate change over the 21st century: Partitioning the effects of nutrients, temperature and light. *Biogeosciences*, *7*(12), 3941–3959. https://doi.org/10.5194/bg-7-3941-2010

Matebr, R. J., & Hirst, A. C. (1999). Climate change feedback on the future oceanic CO_2 uptake. *Tellus B: Chemical and Physical Meteorology*, *51*(3), 722–733.

Mills, M. M., Kropuenske, L. R., Van Dijken, G. L., Alderkamp, A. C., Berg, G. M., Robinson, D. H., et al. (2010). Photophysiology in two Southern Ocean phytoplankton taxa: Photosynthesis of *Phaeocystis antarctica* (Prymnesiophyceae) and *Fragilariopsis cylindrus* (Bacillariophyceae) under simulated mixed-layer irradiance. *Journal of Phycology*, *46*(6), 1114–1127.

Moisan, T., & Fryxell, G. (1993). The distribution of Antarctic diatoms in the Weddell Sea during austral winter. *Botanica Marina*, *36*(6), 489–498.

Moisan, T. A., Olaizola, M., & Mitchell, B. G. (1998). Xanthophyll cycling in *Phaeocystis antarctica*: Changes in cellular fluorescence. *Marine Ecology Progress Series*, *169*, 113–121. https://doi.org/10.3354/meps169113

Moore, J. K., Fu, W., Primeau, F., Britten, G. L., Lindsay, K., Long, M., et al. (2018). Sustained climate warming drives declining marine biological productivity. *Science*, *359*(6380), 1139–1143. https://doi.org/10.1126/science.aao6379

Moreau, S., Mostajir, B., Belanger, S., Schloss, I. R., Vancoppenolle, M., Demers, S., & Ferreyra, G. A. (2015). Climate change enhances primary production in the western Antarctic Peninsula. *Global Change Biology*, *21*(6), 2191–2205. https://doi.org/10.1111/gcb.12878

Nothig, E. M., Bathmann, U., Jennings, J. C., Fahrbach, E., Gradinger, R., Gordon, L. I., & Makarov, R. (1991). Regional relationships between biological and hydrographical properties in the Weddell Gyre in Late Austral Winter 1989. *Marine Chemistry*, *35*(1–4), 325–336.

Oliver, H., St-Laurent, P., Sherrell, R. M., & Yager, P. L. (2019). Modeling iron and light controls on the Summer *Phaeocystis antarctica* bloom in the Amundsen Sea Polynya. *Global Biogeochemical Cycles*, *33*(5), 570–596. https://doi.org/10.1029/2018gb006168

Park, J., Kuzminov, F. I., Bailleul, B., Yang, E. J., Lee, S., Falkowski, P. G., & Gorbunov, M. Y. (2017). Light availability rather than Fe controls the magnitude of massive phytoplankton bloom in the Amundsen Sea polynyas, Antarctica. *Limnology and Oceanography*, *62*(5), 2260–2276. https://doi.org/10.1002/lno.10565

Pasquer, B., Laruelle, G., Becquevort, S., Schoemann, V., Goosse, H., & Lancelot, C. (2005). Linking ocean biogeochemical cycles and ecosystem structure and function: Results of the complex SWAMCO-4 model. *Journal of Sea Research*, *53*(1–2), 93–108. https://doi.org/10.1016/j.seares.2004.07.001

Person, R., Aumont, O., & Lévy, M. (2018). The biological pump and seasonal variability of pCO_2 in the Southern Ocean: Exploring the role of diatom adaptation to low iron. *Journal of Geophysical Research: Oceans*, *123*(5), 3204–3226. https://doi.org/10.1029/2018jc013775

Petrou, K., Kranz, S. A., Trimborn, S., Hassler, C. S., Ameijeiras, S. B., Sackett, O., et al. (2016). Southern Ocean phytoplankton physiology in a changing climate. *Journal of Plant Physiology*, *203*, 135–150.

Rickard, G., & Behrens, E. (2016). CMIP5 Earth system models with biogeochemistry: A Ross Sea assessment. *Antarctic Science*, *28*(5), 327.

Rogers, A. D., Frinault, B. A. V., Barnes, D. K. A., Bindoff, N. L., Downie, R., Ducklow, H. W., et al. (2019). Antarctic futures: An assessment of climate-driven changes in ecosystem structure, function, and service provisioning in the Southern Ocean. *Annual Review of Marine Science*, *12*, 87–120. https://doi.org/10.1146/annurev-marine-010419-011028

Schmidtko, S., Heywood, K. J., Thompson, A. F., & Aoki, S. (2014). Multidecadal warming of Antarctic waters. *Science*, *346*(6214), 1227–1231. https://doi.org/10.1126/science.1256117

Schoemann, V., Becquevort, S., Stefels, J., Rousseau, V., & Lancelot, C. (2005). Phaeocystis blooms in the global ocean and their controlling mechanisms: A review. *Journal of Sea Research*, *53*(1), 43–66. https://doi.org/10.1016/j.seares.2004.01.008

Schofield, O., Miles, T., Alderkamp, A. C., Lee, S., Haskins, C., Rogalsky, E., et al. (2015). In situ phytoplankton distributions in the Amundsen Sea Polynya measured by autonomous gliders. *Elementa-Science of the Anthropocene*, *3*, 1–17. https://doi.org/10.12952/journal.elementa.000073

Schultz, C., Doney, S. C., Zhang, W. G., Regan, H., Holland, P., Meredith, M., & Stammerjohn, S. (2020). Modeling of the influence of sea ice cycle and Langmuir circulation on the upper ocean mixed layer depth and freshwater distribution at the West Antarctic Peninsula. *Journal of Geophysical Research: Oceans*, *125*(8), e2020JC016109. https://doi.org/10.1029/2020JC016109

Sedwick, P. N., DiTullio, G. R., & Mackey, D. J. (2000). Iron and manganese in the Ross Sea, Antarctica: Seasonal iron limitation in Antarctic shelf waters. *Journal of Geophysical Research*, *105*(C5), 11321–11336. https://doi.org/10.1029/2000jc000256

Sedwick, P. N., Garcia, N. S., Riseman, S. F., Marsay, C. M., & DiTullio, G. R. (2007). Evidence for high iron requirements of colonial *Phaeocystis antarctica* at low irradiance. *Biogeochemistry*, *83*(1–3), 83–97. https://doi.org/10.1007/s10533-007-9081-7

Sherrell, R. M., Lagerstrom, M. E., Forsch, K. O., Stammerjohn, S. E., & Yager, P. L. (2015). Dynamics of dissolved iron and other bioactive trace metals (Mn, Ni, Cu, Zn) in the Amundsen Sea Polynya, Antarctica. *Elementa-Science of the Anthropocene*, *3*, 1–27. https://doi.org/10.12952/journal.elementa.000071

Snoek, J., Larochelle, H., & Adams, R. P. (2012). *Practical Bayesian optimization of machine learning algorithms*. Advances in Neural Information Processing Systems 25, pp. 2951–2959.

Solomon, C. M., Lessard, E. J., Keil, R. G., & Foy, M. S. (2003). Characterization of extracellular polymers of *Phaeocystis globosa* and *P. antarctica*. *Marine Ecology Progress Series*, *250*, 81–89.

St-Laurent, P., Yager, P. L., Sherrell, R. M., Oliver, H., Dinniman, M. S., & Stammerjohn, S. E. (2019). Modeling the seasonal cycle of iron and carbon fluxes in the Amundsen Sea Polynya, Antarctica. *Journal of Geophysical Research: Oceans*, *124*, 1544–1565. https://doi.org/10.1029/2018jc014773

St-Laurent, P., Yager, P. L., Sherrell, R. M., Stammerjohn, S. E., & Dinniman, M. S. (2017). Pathways and supply of dissolved iron in the Amundsen Sea (Antarctica). *Journal of Geophysical Research: Oceans*, *122*(9), 7135–7162. https://doi.org/10.1002/2017jc013162

Strzepek, R. F., Boyd, P. W., & Sunda, W. G. (2019). Photosynthetic adaptation to low iron, light, and temperature in Southern Ocean phytoplankton. *Proceedings of the National Academy of Sciences of the United States of America*, *116*(10), 4388–4393.

Strzepek, R. F., & Harrison, P. J. (2004). Photosynthetic architecture differs in coastal and oceanic diatoms. *Nature*, *431*(7009), 689–692. https://doi.org/10.1038/nature02954

Strzepek, R. F., Maldonado, M. T., Hunter, K. A., Frew, R. D., & Boyd, P. W. (2011). Adaptive strategies by Southern Ocean phytoplankton to lessen iron limitation: Uptake of organically complexed iron and reduced cellular iron requirements. *Limnology and Oceanography*, *56*(6), 1983–2002. https://doi.org/10.4319/lo.2011.56.6.1983

Sunda, W. G., & Huntsman, S. A. (1997). Interrelated influence of iron, light and cell size on marine phytoplankton growth. *Nature*, *390*(6658), 389–392.

Sunda, W. G., Swift, D. G., & Huntsman, S. A. (1991). Low iron requirement for growth in oceanic phytoplankton. *Nature*, *351*(6321), 55–57.

Takahashi, T., Sutherland, S. C., Wanninkhof, R., Sweeney, C., Feely, R. A., Chipman, D. W., et al. (2009). Climatological mean and decadal change in surface ocean pCO_2, and net sea-air CO_2 flux over the global oceans. *Deep Sea Research Part II: Topical Studies in Oceanography*, *56*(8–10), 554–577. https://doi.org/10.1016/j.dsr2.2008.12.009

Takahashi, T., Sweeney, C., Hales, B., Chipman, D., Newberger, T., Goddard, J., et al. (2012). The changing carbon cycle in the Southern Ocean. *Oceanography*, *25*(3), 26–37. https://doi.org/10.5670/oceanog.2012.71

Thompson, D. W., & Solomon, S. (2002). Interpretation of recent Southern Hemisphere climate change. *Science*, *296*(5569), 895–899.

Thuróczy, C. E., Alderkamp, A. C., Laan, P., Gerringa, L. J., Mills, M. M., Van Dijken, G. L., et al. (2012). Key role of organic complexation of iron in sustaining phytoplankton blooms in the Pine Island and Amundsen Polynyas (Southern Ocean). *Deep Sea Research Part II. Topical Studies in Oceanography*, *71*, 49–60.

Timmermans, K. R., van der Wagt, B., & de Baar, H. J. W. (2004). Growth rates, half-saturation constants, and silicate, nitrate, and phosphate depletion in relation to iron availability of four large, open-ocean diatoms from the Southern Ocean. *Limnology and Oceanography*, *49*(6), 2141–2151. https://doi.org/10.4319/lo.2004.49.6.2141

Tortell, P. D., Guéguen, C., Long, M. C., Payne, C. D., Lee, P., & DiTullio, G. R. (2011). Spatial variability and temporal dynamics of surface water pCO_2, ΔO_2/Ar and dimethylsulfide in the Ross Sea, Antarctica. *Deep Sea Research Part I: Oceanographic Research Papers*, *58*(3), 241–259. https://doi.org/10.1016/j.dsr.2010.12.006

Treasure, A., Roquet, F., Ansorge, I., Bester, M., Boehme, L., Bornemann, H., et al. (2017). Marine mammals exploring the oceans pole to pole: A review of the MEOP consortium. *Oceanography*, *30*(2), 132–138. https://doi.org/10.5670/oceanog.2017.234

Van De Poll, W. H., Van Leeuwe, M. A., Roggeveld, J., & Buma, A. G. (2005). Nutrient limitation and high irradiance acclimation reduce PAR and UV-induced viability loss in the Antarctic diatom *Chaetoceros brevis* (Bacillariophyceae). *Journal of Phycology*, *41*(4), 840–850.

Van Leeuwe, M., & Stefels, J. (2007). Photosynthetic responses in *Phaeocystis antarctica* towards varying light and iron conditions. In M. A. van Leeuwe, J. Stefels, S. Belviso, C. Lancelot, P. G. Verity, & W. W. C. Gieskes (Eds.), *Phaeocystis, major link in the biogeochemical cycling of climate-relevant elements* (pp. 61–70). Dordrecht: Springer Netherlands. https://doi.org/10.1007/978-1-4020-6214-8_6

van Oijen, T., van Leeuwe, M. A., Gieskes, W. W. C., & de Baar, H. J. W. (2004). Effects of iron limitation on photosynthesis and carbohydrate metabolism in the Antarctic diatom *Chaetoceros brevis* (Bacillariophyceae). *European Journal of Phycology*, *39*(2), 161–171. https://doi.org/10.1080/0967026042000202127

Vernet, M., Sines, K., Chakos, D., Cefarelli, A. O., & Ekern, L. (2011). Impacts on phytoplankton dynamics by free-drifting icebergs in the NW Weddell Sea. *Deep Sea Research Part II: Topical Studies in Oceanography*, *58*(11–12), 1422–1435. https://doi.org/10.1016/j.dsr2.2010.11.022

Wang, S., & Moore, J. K. (2011). Incorporating phaeocystis into a Southern Ocean ecosystem model. *Journal of Geophysical Research*, *116*, C01019. https://doi.org/10.1029/2009jc005817

Waters, R., Van den Enden, R., & Marchant, H. (2000). Summer microbial ecology off East Antarctica (80–150 E): Protistan community structure and bacterial abundance. *Deep Sea Research Part II. Topical Studies in Oceanography*, *47*(12–13), 2401–2435.

Wright, S. W., & van den Enden, R. L. (2000). Phytoplankton community structure and stocks in the East Antarctic marginal ice zone (BROKE survey, January–March 1996) determined by CHEMTAX analysis of HPLC pigment signatures. *Deep Sea Research Part II: Topical Studies in Oceanography*, *47*(12–13), 2363–2400.

Yager, P. L., Sherrell, R. M., Stammerjohn, S. E., Ducklow, H. W., Schofield, O. M. E., Ingall, E. D., et al. (2016). A carbon budget for the Amundsen Sea Polynya, Antarctica: Estimating net community production and export in a highly productive polar ecosystem. *Elementa-Science of the Anthropocene*, *4*, 000140. https://doi.org/10.12952/journal.elementa.000140